Satellite observations and modeling to understand the Lower Mekong River basin streamflow variability

Ibrahim Nourein Mohammed*
Science Applications International Corporation
Hydrological Sciences Laboratory
NASA Goddard Space Flight Center
Mail Code 617.0
Greenbelt, MD 20771
USA
Tel: +1-301-614-6537
Email: ibrahim.Mohammed@nasa.gov
*Corresponding author

John D. Bolten
Hydrological Sciences Laboratory
NASA Goddard Space Flight Center
Mail Code 617
Greenbelt, MD 20771
USA

Raghavan Srinivasan

Spatial Sciences Laboratory

Department of Ecosystem Science and Management

Texas A&M University

College Station, TX 77843

USA

Venkat Lakshmi

School of Earth Ocean and Environment

University of South Carolina

Columbia, SC 29208

USA

Abstract

In this work, we have used the Soil & Water Assessment Tool (SWAT) to examine streamflow variability of the Lower Mekong River Basin (LMRB) associated with changes in the Upper Mekong River Basin (UMRB) inflows. Two hypothetical experiments were formulated and evaluated for the LMRB, where we conducted runoff simulations with multiple inflow changes that include upstream runoff yield increase and decrease scenarios. Streamflow variability of the LMRB was quantified by two streamflow metrics that explain flow variability and predictability, and high flow disturbance. The model experiments were performed for the Lower Mekong River Basin with identical climate, soil, and other watershed characteristics data. Remote sensing precipitation (Tropical Rainfall Measurement Mission, TRMM, and Global Precipitation Measurement mission, GPM), meteorological data as well as spatial data that include a digital elevation model, newly developed soil information (Harmonized World Soil Database, HWSD), and land use and land cover were processed as input to the LMRB model simulations. Observed daily streamflow data along the Lower Mekong River from Chiang Sean, Thailand to Kratie, Cambodia were used for calibration and validation. Our work results suggest that the Lower Mekong River streamflow is highly variable and has a low predictability (Colwell index of about 32%). We found that releasing more water from upstream Mekong during rainfall months by 30% would result in a reduction in the Lower Mekong streamflow predictability by about 21%. This reduction in predictability is mainly attributed to a decrease in the Contingency index. Our work shows that the ability to predict floods/droughts at the Lower Mekong River would be reduced if there is any anticipated change (i.e., increase/decrease) from UMRB releases. Our results also show that releasing more flows from

57 the upstream Mekong would also affect flood duration and the frequency of flood occurrences
58 downstream. The results of this work thus help to quantify the sensitivity of streamflow
59 variability at the Lower Mekong River Basin to upstream anthropogenic changes.
60
61 Keywords: Mekong River; Streamflow variability; Streamflow predictability; Remote
62 sensing; SWAT; Flooding

1. Introduction

Freshwater availability is necessary to promote economic growth through agriculture, fisheries, transport, environmental health, and social equity (Haddeland et al., 2006; Mekong River Commission, 2017; Milly et al., 2005; Veilleux and Anderson, 2016; Wang, 2017; Ziv et al., 2012). Water resources are becoming increasingly limited in availability across the globe. Water shortages may be simplistically attributed to droughts, regulatory cutbacks in deliveries, and demands that outpace new infrastructure and expansion of supply (Grafton et al., 2013; Räsänen et al., 2017; Zhang et al., 2014). Water resources planning efforts are complicated by uncertainty stemming from patterns of economic growth, changes in water use patterns, land use change, and climate change (DeFries and Eshleman, 2004; Dudgeon et al., 2006; Gleick, 2000; Grafton et al., 2013; Jacobs, 2002; Milly et al., 2008; Vörösmarty et al., 2010; Winemiller et al., 2016). While these processes directly increase demands, or decrease supply, research has demonstrated that there are complex processes and dynamic feedbacks among physical processes, biological, biochemical and human-mediated processes that determine change in the water system (Ceola et al., 2014; Heistermann, 2017; Hester and Doyle, 2011; Montanari et al., 2013; Mosley, 2015).

Agriculture is one of the most important aspects to the society and economy and has an enormous impact on the well-being of the countries in the Lower Mekong River Basin (LMRB) such as Vietnam, Thailand, Laos People's Democratic Republic (PDR) and Cambodia (Mainuddin and Kirby, 2009; Mekong River Commission, 2009b). The Mekong River Basin has experienced large variations in precipitation and hence agricultural productivity (Mainuddin and Kirby, 2009). In order to understand these variations over large spatial scales and long-time periods, a

85 better understanding of (i.e., observation and prediction) the hydrologic cycle is necessary –
86 hence use of satellite data and models is warranted (Hoang et al., 2016; Kite, 2001; Lakshmi,
87 2004; Lyon et al., 2017; Piman et al., 2013b; Wang et al., 2016; Wild and Loucks, 2014).
88 The seasonal variations in the Mekong River's flow typically follow a dry season
89 (December to May) and a wet season or a flood season (July to October). The Mekong River
90 streamflow regime changes have been studied in multiple studies (Cochrane et al., 2014;
91 Delgado et al., 2010; Kummu and Sarkkula, 2008; Li et al., 2017; Lu Xi Xi and Grundy-Warr,
92 2008; Mekong River Commission, 2009a; Piman et al., 2013a; Räsänen et al., 2012; Räsänen et
93 al., 2017; Thanh et al., 2015). These studies summarized the observed Mekong River
94 streamflow regime change as streamflow reduction during wet seasons and streamflow
95 increase in dry seasons. Studies cited above have tried to discern the causes for such
96 alterations in the Mekong River streamflow regimes. It has been found that the main causes
97 for streamflow alterations in the Mekong River were attributed to human activities and climate
98 change effects (Hoang et al., 2016; Wang et al., 2017a). Studies on flow regime
99 characterization have been examined via metrics that describe the magnitude, frequency,
100 duration, timing and rate of change for streamflow (Poff, 1996; Poff et al., 1997). Human
101 activities occurring in the Upper Mekong River Basin (UMRB) altering the Mekong flows have
102 recognizable impacts on Lower Mekong streamflow regimes as seen in aquatic ecosystems
103 species, nutrient delivery, water temperatures, riparian livelihoods, sediment movement, and
104 floodplain interactions. Recent studies on the Lower Mekong River highlighted the critical need
105 for specifying and implementing flow regimes to address trade-offs between socioeconomic

106 activities (e.g., fishery), ecological needs, and energy security (Poff and Olden, 2017; Sabo et al.,
107 2017).

108 This work has integrated multiple satellite-based earth observation systems and spatial
109 data with the Soil & Water Assessment Tool (SWAT) hydrologic model employed in the Mekong
110 Basin region to explore water availability, based on both hydrologic flows and total water
111 demands/use using and enhanced remotely sensed products. The scarcity and the
112 incompleteness of many gauge data observations make it imperative to use remote sensing
113 data in modeling the LMRB. From this work, a comprehensive suite of hydrologic data products
114 has been developed and used to improve water accounting and floodplain management using
115 the hydrological cycle variables such as air temperature, evapotranspiration, and precipitation
116 in the LMRB. The main objective of this work is the better understanding of the hydrological
117 cycle of the LMRB, and the floodplain management over the basin. We explore the streamflow
118 variability of the Lower Mekong River by examining the impacts associated with changes in the
119 UMRB inflow. The UMRB inflow to the Lower Mekong changes are generally due to reservoir
120 construction for hydropower development. Overall, our work aims to assess the value-added
121 information of simulating hydrological processes in the LMRB by using a hydrological model
122 (SWAT) with climatological forcing data of satellite-based earth observation as an alternative to
123 scarce in-situ data.

2. Methods

2.1. Study Site

The Mekong River originates in the high altitude of the Tibetan Plateau in China and flows south through five countries (Myanmar, Laos PDR, Thailand, Cambodia, and Vietnam) ending in a large delta before exiting to the South China Sea. The Mekong River Basin is divided into the Upper and the Lower basins. The Lower Mekong River Basin begins when the Mekong River leaves the Chinese province of Yunnan and enters the Golden Triangle where the country borders of Thailand, Laos PDR, China and Myanmar come together (Figure 1).

2.2. Spatial Data

A digital elevation model (DEM) with 1 arc-sec grid resolution for the study area was obtained from the Advanced Spaceborne Thermal Emission and Reflection Radiometer (ASTER) Global Digital Elevation Model (https://doi.org/10.5067/ASTER/ASTGTM.002). The DEM map with 90-meter resolution was used to derive slope and aspect grids for the LMRB model input. The slope class of 2%—8% covers about 40% of the watershed area.

The study area soil information data was obtained from the Harmonized World Soil Database, HWSD (FAO et al., 2012). The LMRB soil texture is mainly sandy clay loam and covers approximately 42% of the basin.

The Land Use/Land Cover (LULC) data was obtained from a 2010 LULC map at a spatial resolution of a 0.25 kilometer for the Lower Mekong Basin using 2010 Moderate Resolution Imaging Spectroradiometer (MODIS) monthly normalized difference vegetation index (NDVI) data as the primary data source (Spruce et al., 2017). The study watershed LULC areas are

145 mainly forest and agricultural lands. The rice crop is farmed on about 26% of the watershed
146 area, while forest land covers constitute about 30% of the watershed area (Spruce et al., 2017).
147 2.3. Meteorological Data
148 Recent works have evaluated the accuracy of satellite-based precipitation in the
149 Mekong River Basin and found that satellite-based precipitation advances hydrological studies
150 in the Mekong region (He et al., 2017; Wang et al., 2017b). For this work, daily cumulative
151 precipitation data was obtained from the Global Precipitation Measurement mission (GPM) and
152 the Tropical Rainfall Measurement Mission (TRMM) remote sensing data and used as inputs for
153 the LMRB model. The Integrated Multi-Satellite Retrievals for GPM (IMERG) dataset used for
154 this work was the GPM_3IMERGDF (https://pmm.nasa.gov/data-access/downloads/gpm).
155 Since IMERG data products are only available from 12 March 2014 to present, then we used the
156 TRMM rainfall data (3B42RT) for time periods earlier than 12-March-2014. A nearest neighbor
157 methodology was used in filling the IMERG data points with the TRMM data points as an
158 approximation during the 01 March 2000 to 11 March 2014 time period, because TRMM and
159 IMERG data do not have the same spatial resolution (i.e., 0.25 and 0.1 degree respectively).
160 Minimum and maximum daily air temperature data was calculated from air temperature
161 record obtained from the Global Land Data Assimilation System (GLDAS) simulation data
162 products (Rodell et al., 2004). For this work, we used the GLDAS_NOAH025_3H.2.1 data
163 products retrieved from https://disc.gsfc.nasa.gov/. Wind speed, relative humidity, and solar
164 radiation data needed for our modeling work were estimated using the global reanalysis
165 weather data from the National Centers for Environmental Prediction (NCEP)
166 http://www.ncep.noaa.gov/, and the Climate Forecast System Reanalysis (CFSR). Aggregated

167 weighted average annual precipitation, and minimum and maximum air temperature time
168 series for the LMRB are shown in Figure 2. A tool (*nasaaccess*) has been developed and
169 presented in Appendix A.2 to access and process remote sensing data obtained from various
170 NASA servers needed for setting up SWAT model or any other rainfall/runoff model.

171 2.4. Flow Regime Metrics

172 In this paper, we examine two streamflow classes and how they change with the UMRB
173 developments at various sites along the LMRB. The streamflow classes studied in this work are
174 flow variability and predictability, and high flow disturbance. A summary of the streamflow
175 regime metrics used to assess UMRB flow change impacts along the LMRB is listed in Table 1.
176 We used the Mann Kendall trend analysis (Helsel and Hirsch, 2002) for trends analyses in flow
177 regime data. Flow variability and predictability streamflow metrics used in this work include a
178 coefficient of variation (*DAYCV*) variable, flow reversals variable (*FLOWREV*), and three flow
179 variables defining the Colwell index which are Predictability (*P*), Constancy (*C*) and Contingency
180 (*M*) (Colwell, 1974). High flow disturbance streamflow metrics used in this work include a flood
181 duration (*FLDDUR*) variable, and a seven-day maximum flow (*7QMAX*) variable. Further details
182 on streamflow classes used are discussed in Appendix A.3.

183 Streamflow data for this work was obtained from the Mekong River Commission (MRC,
184 www.mrcmekong.org). Updated streamflow data was interpolated from recent observed level
185 data obtained from the Asian Preparedness Disaster Center (*ADPC, personal communication*).

186 For this work, we used the rescaled range analysis (R/S) to calculate the *Hurst*
187 (1951) exponent. *Hurst* (1951) observed that the difference between largest surplus
188 and the greatest deficit gives the capacity that a reservoir must have to maintain a

189 constant release equal to the mean of the river without overflows or deficits during the
190 record period years (n). This transitory behavior is widely known as the Hurst
191 phenomenon. *Kottegoda and Rosso* (1997) summarize the rescaled range analysis as:

$$\frac{R^*(n)}{s(n)} = cn^H \quad (1)$$

192 where, $s(n)$ is the standard deviation of the discharge sample of n values, c is a
193 constant equal to $(\pi/2)^{0.5}$, H is the *Hurst* coefficient, $R^*(n)$ is the adjusted range
194 difference between maximum D_n^+ and minimum D_n^- of the accumulated departures
195 from the discharge mean, $\bar{X}_n$. $R^*(n)$ is explained as:

$$R^*(n) = \max_{1\le i\le n}\left(\sum_{j=1}^{i} X_j - i\,\bar{X}_n\right) - \min_{1\le i\le n}\left(\sum_{j=1}^{i} X_j - i\,\bar{X}_n\right) = D_n^+ - |D_n^-| \quad (2).$$

196 2.5. Hydrological Model – SWAT

197 The SWAT is a conceptual watershed-scale hydrological model designed to address
198 water management, sediment, climate change, land use change, and agricultural chemical
199 yields related challenges (Arnold and Fohrer, 2005; Arnold et al., 2012; Arnold et al., 1998;
200 Douglas-Mankin et al., 2010; Gassman et al., 2007; Srinivasan et al., 1998b). The SWAT
201 applications range from field scale to watershed scale (Daggupati et al., 2015) to continental
202 scale (Abbaspour et al., 2015; Srinivasan et al., 1998a). The SWAT model components are
203 hydrology, weather, sedimentation, soil temperature, crop growth, nutrients, pesticides, and
204 agricultural management. The hierarchical structure for modeling units in SWAT is set to be
205 multiple sub-watersheds, which are then further subdivided into hydrologic response units
206 (HRUs) that consist of homogeneous land use, management, and soil characteristics. The SWAT

simulates the overall hydrologic balance for each HRU and model output is available in daily, monthly, and annual time steps. SWAT meteorological inputs include daily precipitation, maximum and minimum temperature, solar radiation, humidity and wind speed. The version of SWAT used in this work is SWAT2012 rev. 635 (Arnold et al., 2013). The Penman–Monteith method was used to simulate potential evapotranspiration for this work. The SWAT Calibration and Uncertainty Procedures (SWAT-CUP) software package with the Sequential Uncertainty Fitting (SUFI2) method (Abbaspour et al., 2007) was used in model calibration. Watershed stream network and sub-basins were generated using the *Arc SWAT* software (http://swat.tamu.edu/software/arcswat/) watershed analysis module (Watershed Delineator) with a contributing area threshold of 253.5 km^2 resulting in 1,138 sub-basins. Applying the HRU module in *Arc SWAT* software with 10% land use percentage over sub-basin area, 10% soil class percentage over land use area, and 10% slope class percentage over soil area, we obtained 10,096 HRUs for the LMRB model.

3. Results

3.1. LMRB Streamflow Statistics

Table 2 gives various statistical measures for the Lower Mekong River annual streamflow using calendar years at different gauges along the main river stem and upstream tributaries. Upper basin inlet streamflow record for the years 2008 and onward, needed for our modeling work, has been regressed from the nearby station (Chiang Sean) streamflow record. The Vientiane (Laos, PDR), station # 011901, the longest monitoring available record compared with other stations studied (1913–2016), has a mean annual streamflow of 4,476 m^3/sec. Minimum, maximum, different quantiles, standard deviation, and coefficient of variation values for annual streamflow at different stations are presented. Streamflow stations skewness values suggest the location and the shape of probability distribution (i.e., positive or negative). In Table 2, we also give the Hurst coefficient (Hurst, 1951; Weron, 2002). The Hurst coefficient is an indicator of a serial correlation or dependence for the annual streamflow time series studied. Across the multiple streamflow stations studied at the lower Mekong the Hurst coefficient for annual flows is greater than 0.5 suggesting that high flows most likely will be followed by another high flow in the future. Multiple works have presented various LMRB streamflow statistics (Lacombe et al., 2014; Rossi et al., 2009). However, Table 2 adds a new information - the coefficient of variation, skewness, and persistence and autocorrelation explained by the Hurst coefficient for the Lower Mekong River.

3.2 Calibration and Validation of the LMRB model

SWAT uses many parameters to describe typical soil, plant growth, land cover, reservoir, and agricultural management characteristics. In this work, the LMRB model was calibrated to

242 daily streamflow and monthly average streamflow at the LMRB sub-basin outlets during the
243 2005 and 2006 with few parameters as outlined in Table 3. Validation of the LMRB model was
244 performed at the LMRB sub-basin outlets during the time period of 2001–2004, and 2007–
245 2015. Parameters used and suggested range values for the LMRB model calibration were
246 consulted and obtained from SWAT developers (*R. Srinivasan, personal communication*) and
247 previous works of *Neitsch et al.*, (2002) and *Rossi et al.*, (2009). All other parameters in the
248 LMRB model were left at their default values. Our LMRB model showed higher sensitivity to
249 parameters related to correction factors for precipitation inputs. In general, we found that
250 running our model without remote sensing precipitation data adjustments tend to
251 overestimate simulated streamflow by about 13%. Therefore, we used a separate precipitation
252 correction factor for each sub-basin watershed.
253 Figure 3 gives observed and simulated daily streamflow at the LMRB (six sub-
254 basins) during the calibration years. The LMRB model is able to explain about 84% of
255 the variance seen in daily streamflow across the Lower Mekong River Basin during the
256 calibration years. In addition, the average percent error (Q_{err}) between daily simulated
257 and observed streamflow across the basin is about 0.86% (Figure 3). We also observe
258 that the Q_{err} and the Nash–Sutcliffe performance metric (NSE) in calibration of our
259 model at monthly results varies between -1.9% and 4.76% and 0.91 and 0.96 for the six
260 sub-basins, respectively (Figure 4). The calibrated value for the soil evaporation
261 compensation factor parameter (ESCO = 0.6) is found to be lower than previous values
262 reported by *Rossi et al.*, (2009) for the LMRB. Generally, as the value for ESCO is
263 reduced the SWAT model is able to extract more of the evaporative demand from lower

soil layers. We argue here that the newer soil data used in this work has influenced a newer value of ESCO for the LMRB different than the default one previously used (i.e., ESCO = 0.95). The parameters listed in Table 3 are among many parameters that describe the SWAT soil physical characteristics and influence the movement of water and air through the soil profile and shallow aquifer underneath it, thus they have a major impact on the cycling of water within the SWAT modeling unit (HRU).

Figure 5 gives monthly observed and simulated streamflow for the study watershed in validation of the LMRB model during 13 years. In general, the model captured the timing of onset and end of seasonal streamflow but was slightly off in some estimates of peak flows. The NSE metric during validation time period for our model varies between 0.86 and 0.95. The model has about 3.85% error on average in estimating monthly flows during the validation time period. Our LMRB model evaluation results are similar to previous attempts presented by *Rossi et al.,* (2009) who reported a Nash-Sutcliffe flow monthly efficiency values ranging between 0.8 and 1.0 at mainstream monitoring stations.

3.3 LMRB Flow Regime

In this study, the experiment we performed covered the LMRB model scenario analyses. Hypothetical scenarios of reducing and increasing the UMRB flow inputs during June, July, August, and September months by up to 30% of the existing flows conditions have been examined and tracked downstream. Lower Mekong flow records at these specific months (June, July, August, and September) are usually very high

285 compared with other flow records during the year (Figure 6). Figure 6 gives the
286 streamflow daily variation at Vientiane (Sub-basin 3) during 1913 to 2016.
287 The Mekong River historical streamflow data suggests that the river has a high
288 streamflow variability. The *DAYCV* at Sub-basin 7 and Sub-basin 8 river sections varies
289 between 117% to 154%. Results showed that the downstream river section Sub-basin 6
290 has a higher *DAYCV* compared with upstream river section Sub-basin 1 (Table 4). We
291 attribute this phenomenon to the fact that the Mekong River is a highly regulated river
292 system with many reservoirs that have different operation plans. This complexity in
293 managing the river sections has resulted in a trend of *DAYCV* increase as we move
294 downstream the Mekong River. Upon examination of the streamflow variability
295 (*DAYCV*) with changes in upstream releases to the Lower Mekong, we found that flow
296 variability is pronounced at SB1 and decreases as we go downstream till SB6. Sub-basin
297 1 *DAYCV* varies between 20% to -2%, while Sub-basin 6 *DAYCV* varies between 1-2%
298 (Table 4). We infer here that the streamflow coefficient of variation changes would be
299 clearly seen at the upper part of the Lower Mekong specially when more flows are
300 released from the upstream Mekong River.
301 Analysis of the Lower Mekong River historical streamflow data during 2001–2015
302 using the Colwell index metrics indicates that the flow has a low predictability (average
303 of $P \approx 32\%$). The Constancy (*C*) at the observed historical predictability is on average of
304 26%. This suggests that the Mekong River streamflow gauges predictability are due to
305 high constancy of streamflow which varies little among months and years studied
306 (Figure 7 and Figure 8). Therefore, the streamflow discharge at the Lower Mekong

307 (which never varies across seasons during years studied) is perfectly predictable with all
308 the predictability deriving from the constancy component.

309 Upon changing the inflow input from upstream, the downstream streamflow
310 predictability has been reduced further. In Figure 7, we give at three sub-basins (SB4,
311 SB5, and SB6) the percent change in predictability (*P*) as a result of upstream input flow
312 changes. We realize that any change in input flow, whether it is increase or decrease in
313 input flow, reduces the predictability at the LMRB. However, upstream input flow
314 increases affect the Colwell predictability more than upstream input flow decreases.
315 This corroborates with the expected flooding in LMRB as a result of upstream higher
316 input flows. For example, in Figure 7, SB4 sensitivity results (top panel) suggests that
317 increasing the upstream flow by 30% more than existing current conditions would result
318 in reducing the predictability (*P*) by about 33% to be 0.23 (current *P* at SB4 is equal to
319 0.34).

320 Looking at Kratie, Cambodia (SB6) in Figure 8, we see that releasing more water
321 from upstream Mekong during raining months by 30% would mean a reduction in
322 predictability by 21%. This reduction in predictability is mainly attributed to a reduction
323 in the Contingency index. Since Contingency represents the degree to which time
324 determines state, or the degree to which they are dependent on each other. This can
325 be translated to a change in flooding occurrence times. This streamflow predictability
326 findings can be generalized at the whole Lower Mekong by saying that our ability to
327 predict floods/droughts in general would be reduced if there is any change (i.e.,
328 increase/decrease) anticipated from upstream Mekong releases.

329 The other streamflow variability pattern we studied in this work was flow
330 reversals (*FLOWREV*). We found that flow reversals are showing a notable increasing
331 trend across the LMRB (Figure 9). We think that this observation of striking increase in
332 flow reversal days is mainly due to the effect of flow regulations in the Mekong River
333 Basin (Upper and Lower). Upon examining flow reversals trends when input releases
334 from upstream Mekong are changed, we found that in general flow reversal days are
335 increasing. This means a higher flow variability would be experienced upon changing
336 input releases.
337 Our analysis of high flow disturbance for the Lower Mekong River streamflow
338 regime covered seven-day maximum flow and flood duration variables. Mann Kendall
339 trend analysis for seven-day maximum flow (*7QMAX*) was used to examine whether any
340 trends in maximum flows were statistically significant. Table 5 gives Mann Kendall trend
341 analysis results for the historic seven-day maximum flow as well as seven-day maximum
342 flow when input flow releases from upstream Mekong were adjusted. In general, we
343 found that there is decreasing trend of *7QMAX* across the whole lower Mekong during
344 time period studied (e.g., 2001-2015) with an average *7QMAX* value varies from 3 to 6
345 millimeters per day at Sub-basin 1 and Sub-basin 6. We correlate the observed
346 decreasing trend of *7QMAX* and the increasing trend of *7QMIN* (results not shown) to
347 the increased number of flow reversals seen earlier in Figure 9. That means increased
348 number of flow reversals are increased number of days with low flow changes.
349 Another high flow disturbance variable studied in this work was flood duration
350 (*FLDDUR*). Generally, flood durations within the LMRB are long and more frequent

specially at Mukdahan, Thailand and southward (Figure 10). For instance, on 2011 the streamflow gauge discharge record at Mukdahan recorded 13 days with discharges equal to or exceed a threshold of 30,400 m^3/sec (equivalent to 12.6 meters as a stage height). Our results reveal that releasing more flows from the UMRB (i.e., 30% increase) at the same year of 2011, would have caused the same streamflow gauge to record 16 days of discharges equal to or exceed the flood threshold. Our results also show that releasing more flows from the UMRB would also affect the frequency of flood occurrences. Therefore, changing flow releases from upstream Mekong need to be carefully examined since not only flood duration is going to change but also flood occurrences is going to change too.

4. Discussion

SWAT is the choice of watershed model by many stakeholders in the Mekong Basin region for their decision framework, including the Mekong River Commission, and has been identified in the SERVIR-Mekong Regional Needs Assessment (NASA, 2014). We have used multiple satellite-based earth observation systems and a spatial data to build up a hydrologic model (SWAT) for the Lower Mekong River Basin. Our objective to develop a physically based hydrological model at the LMRB was to better understand the impacts associated with UMRB water changes on the LMRB streamflow variability, and flood frequency and duration. Multiple streamflow regime variables were examined across the Lower Mekong under different scenarios of UMRB water releases. Our modeling efforts presented are thought to be in line with a substantial body of literature that discusses the Lower Mekong River hydrological change under expected and on-going hydropower development and climate change effects (Li et al., 2017; Lyon et al., 2017; Piman et al., 2016; Piman et al., 2013b). Growing populations, and the staggering effects of climate change that are seen in high temperatures, and variable precipitation patterns over the Mekong River raise the potential for shifts in the hydrological responses at the Lower Mekong Basin. Having updated statistics on streamflow information at the LMRB is then needed given the ongoing regional development occurring at the basin in terms of agricultural expansion and infrastructure development.

The Lower Mekong flow variability and predictability conditions will be directly affected in terms of increased flow variability and decreased flow predictability due to

383 changing input flow releases from the UMRB. Releasing more water from the UMRB
384 during rainy season (for instance by 30%) would imply a further reduction in the Lower
385 Mekong streamflow predictability (i.e., Colwell index reduces to 25%). Stream
386 ecologists such as *Resh et al.*, (1988) and *Lazzaro et al.*, (2013) are often interested in
387 studying streamflow regime because of its relation to channel disturbance. Our work
388 suggested that flow releases increase from the UMRB would mean more flooded days as
389 well as higher frequency of flood occurrences specially at Mukdahan (Thailand), Pakse
390 (Laos), and Kratie (Cambodia). This is an alarming finding since the fate of many people
391 and properties will be at stake.

392 Models results are often uncertain. The model simulation efficiencies have to be
393 considered in examining the results of this work. The uncertainty and limitations seen
394 are due to the nature of modelling that could be related to error in model data inputs,
395 parameters and process representation. It is worth to mention here that the LMRB
396 models' performance comparison was based on monthly flows output, so some amount
397 of temporal and spatial aggregation may have masked individual event prediction or
398 adds uncertainty. We do agree that model results such as the ones presented in this
399 work should be thought and considered as tools used to efficiently and collaboratively
400 guide decision makers. In conclusion, collaborative work and sharing information
401 between the upstream and downstream Mekong River agencies and stakeholders is
402 critically needed to successfully manage the precious Mekong River. Remote sensing
403 data can aide and has achieved a nice job in addressing hydrologic modeling needs and
404 requirements at the Lower Mekong River Basin.

5. Acknowledgements

This work was fully supported by the National Aeronautics and Space Administration (NASA), Goddard Space Flight Center (GSFC) Applied Sciences Grants NNX16AT88G, NNX16AT86G, and NNG15HQ01C. Special thanks are extended to Joe Spruce who processed and shared with us the Land Use/Land Cover map for the Lower Mekong Basin. Any opinions, findings, and conclusions or recommendations expressed in this work are those of the author(s) and do not necessarily reflect the views of the National Aeronautics and Space Agency, Science Systems and Applications, Inc., and Science Applications International Corporation.

6. Appendix

A.1. Dams Data

Data for existing dams within the Mekong Basin was obtained from the Greater Mekong Consultative Group for International Agricultural Research (CGIAR) Program on Water, Land and Ecosystems (WLE, 2017). In Figure 1, we depict dams within the Lower Mekong River Basin that are either already commissioned or still under construction and have a maximum reservoir area greater than or equal to 280 km^2 similar to the MRC SWAT model setup. The surface area of the reservoirs behind the various dams that we have included in this study are listed in Table A. 1.

A.2. nasaaccess

The 'nasaaccess' package with R software (R Development Core Team, 2017) current version (*nasaaccess* version 1.2) processes remote sensing data products (i.e., TRMM, GPM, and GLDAS) and creates weather input definition tables as well as stations data files in a format readable by SWAT model or any other rainfall/runoff model. The *nasaaccess* package can be expanded to include other remote sensing products needed in future. For the time being, *nasaaccess* generates daily rainfall and minimum and maximum air temperatures gridded data and gridded data definition files needed to serve as a setup for any basic SWAT/other model run. The core functionality of the *nasaaccess* package access NASA Goddard Space Flight Center (GSFC) servers to download climate data, clip needed grids based on a user study watershed, handles temporal issues (e.g., GLDAS product has 3-hour temporal resolution), and then generates daily climate gridded data files and definition files compatible with SWAT/other models. The inputs needed for the various functions within the *nasaaccess* are: start and end dates for a user climate data simulation period, and a shapefile and a DEM grid for a study watershed.

A.3. streamflow regime metrics

The coefficient of variation variable (*DAYCV*) is defined as the standard deviation of daily flows divided by the average of daily flows multiplied by 100 during a year. The annual coefficient of variation can be expressed as:

$$DAYCV = \frac{\sigma}{\mu} \times 100\,, \tag{A.3.1}$$

where σ is the unbiased standard deviation (denominator is $n-1$), and μ is the arithmetic mean during a year of flow records. The *DAYCV* describes overall the flow variability regardless of sequential flow variations. Generally, flow variability is lower in downstream than upstream river sections (Horwitz, 1978).

Flow reversals (*FLOWREV*) are defined here from the daily streamflow as days when the trend (increasing or decreasing) from the previous days is reversed. Flow reversals are calculated by counting the days when flow records are higher (rising) or lower (falling) than previous day records. This can be explained as:

$$FLOWREV\ is\ counted\ when$$
$$\begin{cases} sign(DQ_j)\ is\ positive\ \&\ sign(DQ_{j-1})\ is\ zero\ or\ negative \\ sign(DQ_j)\ is\ negative\ \&\ sign(DQ_{j-1})\ is\ zero\ or\ positive \end{cases}, \tag{A.3.2}$$

where $DQ = diff(Q)$, $diff(Q)$ is flow lagged differences, and Q is a daily flow vector, and $sign(DQ_j)$ is the sign of the corresponding element in lagged difference vector DQ.

Colwell's indices (Colwell, 1974) are flow predictability metrics developed to assess relevant measures of flow variability (e.g., biological). The principal value of the Colwell index used in our work is for comparison of the uncertainty of the variable river environment projected due to upper stream changes. The Colwell procedure is

457 analogous to autocorrelation analysis and to some aspects of harmonic analysis. The
458 Colwell's predictability (P) is the sum of constancy (C) and contingency (M).
459 Constancy (C) is a measure of temporal invariance, and contingency (M) is a measure
460 of periodicity. Constancy is defined similar to predictability, except that seasonal
461 variability across periods is disregarded. Contingency is defined as the degree to which
462 time period and value group are dependent on each other. The P, C, and M are scaled
463 to range from 0 to 1. Further details on Colwell index are presented at Appendix B in
464 *Mohammed et al.* (2015).

465 Calculation of Colwell's indices requires that streamflow values be binned into
466 discrete groups. As with all information measures absolute values are dependent on
467 this binning, but a consistent binning allows relative comparisons. Following
468 *Mohammed et al.* (2015) and others, we used 7 bins $(< 0.5\ \mu, 1.0\ \mu, 1.5\ \mu, 2.5\ \mu, 3.0\ \mu, >$
469 $3.0\ \mu)$, where μ is equal to the mean of daily streamflow values, to define groups for dry
470 and flood seasons of the streamflow record. These two seasons represent the seasonal
471 cycle for the LMRB and we counted the number of occurrences of daily streamflow
472 values in states defined by groups (bins) and periods (seasons) to arrive at the Colwell's
473 indices. Dry season time period is from January 1st to May 31st and flood season time
474 period is from June 1st to December 31st. Following Colwell, for a frequency matrix
475 (contingency table) with t columns (times within a cycle) and s rows (state of the
476 phenomenon). Let N_{ij} be the number of cycles for which the phenomenon was in state
477 i at time j. Define the column totals (X_j), row totals (Y_i), and the grand total (Z) as:

$$X_j = \sum_{i=1}^{s} N_{ij}\,, Y_i = \sum_{j=1}^{t} N_{ij}\,, and\ Z = \sum_i \sum_j N_{ij} = \sum_j X_j = \sum_i Y_i \qquad \text{(A.3.3).}$$

478 Then, the uncertainty with respect to time is:

$$H(X) = -\sum_{j=1}^{t} \frac{X_j}{Z} log \frac{X_j}{Z} \qquad \text{(A.3.4),}$$

479 the uncertainty with respect to state is:

$$H(Y) = -\sum_{i=1}^{s} \frac{Y_i}{Z} log \frac{Y_i}{Z} \qquad \text{(A.3.5),}$$

480 and the uncertainty with respect to the interaction of time and state is:

$$H(XY) = -\sum_i \sum_j \frac{N_{ij}}{Z} log \frac{N_{ij}}{Z} \qquad \text{(A.3.6).}$$

481 The predictability of a periodic phenomenon is maximal when there is complete
482 certainty with regard to state (row) once the point in time (column) is specified. In
483 terms of information theory, the conditional uncertainty with regard to state, with time
484 given, is defined as: $H_X(Y) = H(XY) - H(X)$ (Jelínek, 1968). When predictability is at
485 its minimum, all states are equiprobable for all times. In this case $H(X) = \log t$, and
486 $H(XY) = \log st$, so that $H_X(Y) = \log s$. To obtain measure of predictability (P) with
487 the range $(0,1)$, define:

$$P = 1 - \frac{H_X(Y)}{\log s} = 1 - \frac{H(XY) - H(X)}{\log s} \qquad \text{(A.3.7).}$$

488 Constancy is maximized when all row totals equal to zero with the exception of a
489 single row total being greater than zero; it is minimized when all row totals are equal.

Since $H(Y)$ varies in precisely the opposite way, and its maximum value is *log s*, a measure of constancy (C) with range $(0,1)$ is given by:

$$C = 1 - \frac{H(XY)}{\log s} \quad \text{(A.3.8).}$$

Contingency represents the degree to which time determines state, or the degree to which they are dependent on each other. In information theory, contingency is measured by a quantity called average mutual information (Jelínek, 1968). *Colwell* (1974) cites contingency as the average amount of information about the state of the phenomenon provided by time or $I(XY) = H(Y) - H_X(Y) = H(Y) + H(X) - H(XY)$. *Colwell* (1974) gives an adjusted measure of contingency (M), with range $(0,1)$ as:

$$M = \frac{H(X) + H(Y) - H(XY)}{\log s} \quad \text{(A.3.9).}$$

Flood duration (*FLDDUR*) is usually calculated as the average number of days per year when flow equals or exceeds flood threshold flow. Since the LMRB is a complex system, estimating the magnitude of daily return flow that we can use in calculating flood duration periods is quite challenging. Upon compilation of several MRC weekly flood situation reports (http://ffw.mrcmekong.org/), we extracted the flood stage height threshold and then estimated the daily return flow using the stage-flow relation along the LMRB. The flood stage heights along the LMRB are: 11.8 meters at Chiang Sean (station # 010501), 18 meters at Luang Prabang (station # 011201), 12.6 meters at Vientiane (station #011901), 12.6 meters Mukdahan (station # 013402), 12.0 meters at Pakse (station # 013901), and 23.0 meters at Kratie (station # 014901). These stage heights correspond to the following flows 18,535; 17,950; 22,399; 30,400; 38,930;

58,256 m^3/sec respectively. We used these flood thresholds at each sub-basin outlet to calculate flood duration periods for this work.

Seven-day maximum flow (*7QMAX*) is the average across years of 7-day maximum streamflow. For each year in the period of record, the maximum 7-day mean is found from the daily mean streamflow and the maximum is the 7-day maximum flow for that year.

7. References

Abbaspour, K.C., Rouholahnejad, E., Vaghefi, S., Srinivasan, R., Yang, H., Kløve, B., 2015. A continental-scale hydrology and water quality model for Europe: Calibration and uncertainty of a high-resolution large-scale SWAT model. J. Hydrol. 524, 733-752, http://dx.doi.org/10.1016/j.jhydrol.2015.03.027

Abbaspour, K.C., Yang, J., Maximov, I., Siber, R., Bogner, K., Mieleitner, J., Zobrist, J., Srinivasan, R., 2007. Modelling hydrology and water quality in the pre-alpine/alpine Thur watershed using SWAT. J. Hydrol. 333, 413-430, https://doi.org/10.1016/j.jhydrol.2006.09.014

Arnold, J.G., Fohrer, N., 2005. SWAT2000: Current capabilities and research opportunities in applied watershed modelling. Hydrol. Process. 19, 563-572, http://dx.doi.org/10.1002/hyp.5611

Arnold, J.G., Kiniry, J.R., Srinivasan, R., Williams, J.R., Haney, E.B., Neitsch, S.L., 2013. SWAT 2012 Input/Output documentation. TR-439, Texas Water Resources Institute, College Station, TX.

Arnold, J.G., Moriasi, D.N., Gassman, P.W., Abbaspour, K.C., White, M.J., Srinivasan, R., Santhi, C., Harmel, R.D., Griensven, A.v., Liew, M.W.V., Kannan, N., Jha, M.K., 2012. SWAT: Model use, calibration, and validation. T ASABE 55, 1491-1508, http://dx.doi.org/10.13031/2013.42256

Arnold, J.G., Srinivasan, R., Muttiah, R.S., Williams, J.R., 1998. Large area hydrologic modeling and assessment part I: Model development. J. Am. Water Resour. As. 34, 73-89, http://dx.doi.org/10.1111/j.1752-1688.1998.tb05961.x

Ceola, S., Montanari, A., Koutsoyiannis, D., 2014. Toward a theoretical framework for integrated modeling of hydrological change. Wiley Interdisciplinary Reviews: Water 1, 427-438, http://dx.doi.org/10.1002/wat2.1038

Cochrane, T.A., Arias, M.E., Piman, T., 2014. Historical impact of water infrastructure on water levels of the Mekong River and the Tonle Sap system. Hydrol. Earth Syst. Sci. 18, 4529-4541, http://dx.doi.org/10.5194/hess-18-4529-2014

543 Colwell, R.K., 1974. Predictability, constancy, and contingency of periodic phenomena.
544 Ecology 55, 1148-1153, http://dx.doi.org/10.2307/1940366

545 Daggupati, P., Yen, H., White, M.J., Srinivasan, R., Arnold, J.G., Keitzer, C.S., Sowa, S.P.,
546 2015. Impact of model development, calibration and validation decisions on
547 hydrological simulations in West Lake Erie Basin. Hydrol. Process. 29, 5307-5320,
548 http:https://dx.doi.org/10.1002/hyp.10536

549 DeFries, R., Eshleman, K.N., 2004. Land-use change and hydrologic processes: A major
550 focus for the future. Hydrol. Process. 18, 2183-2186,
551 http://dx.doi.org/10.1002/hyp.5584

552 Delgado, J.M., Apel, H., Merz, B., 2010. Flood trends and variability in the Mekong River.
553 Hydrol. Earth Syst. Sci. 14, 407-418, http://dx.doi.org/10.5194/hess-14-407-2010

554 Douglas-Mankin, K.R., Srinivasan, R., Arnold, J.G., 2010. Soil and Water Assessment Tool
555 (SWAT) model: Current developments and applications. T ASABE 53, 1423-1431,
556 http://dx.doi.org/10.13031/2013.34915

557 Dudgeon, D., Arthington, A.H., Gessner, M.O., Kawabata, Z.-I., Knowler, D.J., Lévêque, C.,
558 Naiman, R.J., Prieur-Richard, A.-H., Soto, D., Stiassny, M.L.J., Sullivan, C.A., 2006.
559 Freshwater biodiversity: importance, threats, status and conservation
560 challenges. Biol. Rev. 81, 163-182,
561 http://dx.doi.org/10.1017/S1464793105006950

562 FAO, IIASA, ISRIC-World Soil Information, Institute of Soil Science, Chinese Academy of
563 Sciences (ISSCAS), Joint Research Centre of the European Commission (JRC),
564 Harmonized World Soil Database, v1.21, 2012. http://www.fao.org/soils-
565 portal/soil-survey/soil-maps-and-databases/harmonized-world-soil-database-
566 v12/en/

567 Gassman, P.W., Reyes, M.R., Green, C.H., Arnold, J.G., 2007. The soil and water
568 assessment tool: Historical development, applications, and future research
569 directions. T ASABE 50, 1211-1250, http://dx.doi.org/10.13031/2013.23637

570 Gleick, P.H., 2000. A Look at twenty-first century water resources development. Water
571 Int. 25, 127-138, http://dx.doi.org/10.1080/02508060008686804

572 Grafton, R.Q., Pittock, J., Davis, R., Williams, J., Fu, G., Warburton, M., Udall, B.,
573 McKenzie, R., Yu, X., Che, N., Connell, D., Jiang, Q., Kompas, T., Lynch, A., Norris,
574 R., Possingham, H., Quiggin, J., 2013. Global insights into water resources,
575 climate change and governance. Nat. Clim. Change 3, 315-321,
576 http://dx.doi.org/10.1038/nclimate1746

577 Haddeland, I., Lettenmaier, D.P., Skaugen, T., 2006. Effects of irrigation on the water and
578 energy balances of the Colorado and Mekong river basins. J. Hydrol. 324, 210-
579 223, http://dx.doi.org/10.1016/j.jhydrol.2005.09.028

580 He, Z., Yang, L., Tian, F., Ni, G., Hou, A., Lu, H., 2017. Intercomparisons of rainfall
581 estimates from TRMM and GPM multisatellite products over the Upper Mekong
582 River Basin. J. Hydrometeorol. 18, 413-430, http://dx.doi.org/10.1175/jhm-d-16-
583 0198.1

584 Heistermann, M., 2017. HESS opinions: A planetary boundary on freshwater use is
585 misleading. Hydrol. Earth Syst. Sci. 21, 3455-3461,
586 http://dx.doi.org/10.5194/hess-21-3455-2017

587 Helsel, D.R., Hirsch, R.M., 2002. Statistical Methods in Water Resources, Techniques of
588 Water-Resources Investigations of the United States Geological Survey Book 4,
589 Hydrologic Analysis and Interpretation. U.S. Geol. Sur., Reston, VA, pp. 522.

590 Hester, E.T., Doyle, M.W., 2011. Human impacts to river temperature and their effects
591 on biological processes: A quantitative synthesis. J. Am. Water Resour. As. 47,
592 571-587, http://dx.doi.org/10.1111/j.1752-1688.2011.00525.x

593 Hoang, L.P., Lauri, H., Kummu, M., Koponen, J., van Vliet, M.T.H., Supit, I., Leemans, R.,
594 Kabat, P., Ludwig, F., 2016. Mekong River flow and hydrological extremes under
595 climate change. Hydrol. Earth Syst. Sci. 20, 3027-3041,
596 http://dx.doi.org/10.5194/hess-20-3027-2016

597 Horwitz, R.J., 1978. Temporal variability patterns and the distributional patterns of
598 stream fishes. Ecol. Monogr. 48, 307-321, http://dx.doi.org/10.2307/2937233

599 Hurst, H.E., 1951. Long-term storage capacity of reservoirs. T. Am. Soc. Civ. Eng. 116,
600 770-808

601 Jacobs, J.W., 2002. The Mekong River Commission: Transboundary water resources
602 planning and regional security. Geogr. J. 168, 354-364,
603 http://dx.doi.org/10.1111/j.0016-7398.2002.00061.x

604 Jelínek, F., 1968. Probabilistic Information Theory: Discrete and Memoryless Models.
605 McGraw-Hill, New York, 609 pp.

606 Kite, G., 2001. Modelling the Mekong: Hydrological simulation for environmental impact
607 studies. J. Hydrol. 253, 1-13, https://doi.org/10.1016/S0022-1694(01)00396-1

608 Kottegoda, N.T., Rosso, R., 1997. Probability, Statistics, and Reliability for Civil and
609 Environmental Engineers. McGraw-Hill, New York, 735 pp.

610 Kummu, M., Sarkkula, J., 2008. Impact of the Mekong River flow alteration on the Tonle
611 Sap flood pulse. AMBIO 37, 185-192, http://dx.doi.org/10.1579/0044-
612 7447(2008)37[185:IOTMRF]2.0.CO;2

613 Lacombe, G., Douangsavanh, S., Vogel, R.M., McCartney, M., Chemin, Y., Rebelo, L.-M.,
614 Sotoukee, T., 2014. Multivariate power-law models for streamflow prediction in
615 the Mekong Basin. J. Hydrol. Reg. St. 2, 35-48,
616 http://dx.doi.org/10.1016/j.ejrh.2014.08.002

617 Lakshmi, V., 2004. The role of satellite remote sensing in the prediction of ungauged
618 basins. Hydrol. Process. 18, 1029-1034, http://dx.doi.org/10.1002/hyp.5520

619 Lazzaro, G., Basso, S., Schirmer, M., Botter, G., 2013. Water management strategies for
620 run-of-river power plants: Profitability and hydrologic impact between the intake
621 and the outflow. Water Resour. Res. 49, 8285-8298,
622 http://dx.doi.org/10.1002/2013wr014210

623 Li, D., Long, D., Zhao, J., Lu, H., Hong, Y., 2017. Observed changes in flow regimes in the
624 Mekong River Basin. J. Hydrol. 551, 217-232,
625 http://dx.doi.org/10.1016/j.jhydrol.2017.05.061

626 Lu Xi Xi, W.J.-J., Grundy-Warr, C., 2008. Are the Chinese dams to be blamed for the
627 lower water levels in the Lower Mekong? In: Kummu, M., Keskinen, M., Varis, O.
628 (Eds.), Modern Myths of the Mekong : A critical review of water and

development concepts, principles and policies. Water and development publications, 01. Helsinki University of Technology, Espoo, Finland, pp. 39-51.

Lyon, S.W., King, K., Polpanich, O.-u., Lacombe, G., 2017. Assessing hydrologic changes across the Lower Mekong Basin. J. Hydrol. Reg. St. 12, 303-314, http://dx.doi.org/10.1016/j.ejrh.2017.06.007

Mainuddin, M., Kirby, M., 2009. Agricultural productivity in the Lower Mekong Basin: Trends and future prospects for food security. Food Secur. 1, 71-82, http://dx.doi.org/10.1007/s12571-008-0004-9

Mekong River Commission, 2009a. The Flow of the Mekong. No. 2, Mekong River Commission Secretariat,, Vientiane, Lao PDR.

Mekong River Commission, 2009b. MRC's Role in Agriculture and Agricultural Water Management, Mekong River Commission Secretariat,, Vientiane, Lao PDR.

Mekong River Commission, 2017. Transboundary water resources management issues in the Mekong Delta of Cambodia and Viet Nam, Mekong River Commission Secretariat,, Vientiane, Lao PDR.

Milly, P.C.D., Betancourt, J., Falkenmark, M., Hirsch, R.M., Kundzewicz, Z.W., Lettenmaier, D.P., Stouffer, R.J., 2008. Stationarity is dead: Whither water management? Science 319, 573-574, http://dx.doi.org/10.1126/science.1151915

Milly, P.C.D., Dunne, K.A., Vecchia, A.V., 2005. Global pattern of trends in streamflow and water availability in a changing climate. Nature 438, 347-350, http://dx.doi.org/10.1038/nature04312

Mohammed, I.N., Bomblies, A., Wemple, B.C., 2015. The use of CMIP5 data to simulate climate change impacts on flow regime within the Lake Champlain Basin. J. Hydrol. Reg. St. 3, 160-186, http://dx.doi.org/10.1016/j.ejrh.2015.01.002

Montanari, A., Young, G., Savenije, H.H.G., Hughes, D., Wagener, T., Ren, L.L., Koutsoyiannis, D., Cudennec, C., Toth, E., Grimaldi, S., Blöschl, G., Sivapalan, M., Beven, K., Gupta, H., Hipsey, M., Schaefli, B., Arheimer, B., Boegh, E., Schymanski, S.J., Di Baldassarre, G., Yu, B., Hubert, P., Huang, Y., Schumann, A., Post, D.A., Srinivasan, V., Harman, C., Thompson, S., Rogger, M., Viglione, A.,

McMillan, H., Characklis, G., Pang, Z., Belyaev, V., 2013. "Panta Rhei—Everything Flows": Change in hydrology and society—The IAHS Scientific Decade 2013–2022. Hydrolog. Sci. J. 58, 1256-1275, http://dx.doi.org/10.1080/02626667.2013.809088

Mosley, L.M., 2015. Drought impacts on the water quality of freshwater systems; Review and integration. Earth-Sci. Rev. 140, 203-214, http://dx.doi.org/10.1016/j.earscirev.2014.11.010

NASA, 2014. SERVIR Annual Report, United States Agency for International Development and the National Aeronautics and Space Administration, Huntsville, AL.

Neitsch, S.L., Arnold, J.G., Kiniry, J.R., Williams, J.R., King, K.W., 2002. Soil and Water Assessment Tool theoretical documentation version 2000. TR-191, Texas Water Resources Institute, College Station, TX.

Piman, T., Cochrane, T.A., Arias, M.E., 2016. Effect of Proposed Large Dams on Water Flows and Hydropower Production in the Sekong, Sesan and Srepok Rivers of the Mekong Basin. River Res. Appl. 32, 2095-2108, http://dx.doi.org/10.1002/rra.3045

Piman, T., Cochrane, T.A., Arias, M.E., Green, A., Dat, N.D., 2013a. Assessment of flow changes from hydropower development and operations in Sekong, Sesan, and Srepok Rivers of the Mekong Basin. J. Water Res. Plan. Man. 139, 723-732, http://dx.doi.org/10.1061/(ASCE)WR.1943-5452.0000286

Piman, T., Lennaerts, T., Southalack, P., 2013b. Assessment of hydrological changes in the Lower Mekong Basin from Basin-Wide development scenarios. Hydrol. Process. 27, 2115-2125, http://dx.doi.org/10.1002/hyp.9764

Poff, N., 1996. A hydrogeography of unregulated streams in the United States and an examination of scale-dependence in some hydrological descriptors. Freshwater Biol. 36, 71-79, http://dx.doi.org/10.1046/j.1365-2427.1996.00073.x

Poff, N.L., Allan, J.D., Bain, M.B., Karr, J.R., Prestegaard, K.L., Richter, B.D., Sparks, R.E., Stromberg, J.C., 1997. The natural flow regime. BioScience 47, 769-784, http://dx.doi.org/10.2307/1313099

687 Poff, N.L., Olden, J.D., 2017. Can dams be designed for sustainability? Science 358, 1252-
688 1253, http://dx.doi.org/10.1126/science.aaq1422

689 R Development Core Team, 2017. R: A language and environment for statistical
690 computing. R Found. for Stat. Comput., Vienna, Austria.

691 Räsänen, T.A., Koponen, J., Lauri, H., Kummu, M., 2012. Downstream hydrological
692 impacts of hydropower development in the Upper Mekong Basin. Water Resour.
693 Manag. 26, 3495-3513, http://dx.doi.org/10.1007/s11269-012-0087-0

694 Räsänen, T.A., Someth, P., Lauri, H., Koponen, J., Sarkkula, J., Kummu, M., 2017.
695 Observed river discharge changes due to hydropower operations in the Upper
696 Mekong Basin. J. Hydrol. 545, 28-41,
697 http://dx.doi.org/10.1016/j.jhydrol.2016.12.023

698 Resh, V.H., Brown, A.V., Covich, A.P., Gurtz, M.E., Li, H.W., Minshall, G.W., Reice, S.R.,
699 Sheldon, A.L., Wallace, J.B., Wissmar, R.C., 1988. The role of disturbance in
700 stream ecology. J. N. Am. Benthol. Soc. 7, 433-455,
701 http://dx.doi.org/10.2307/1467300

702 Rodell, M., Houser, P.R., Jambor, U., Gottschalck, J., Mitchell, K., Meng, C.-J., Arsenault,
703 K., Cosgrove, B., Radakovich, J., Bosilovich, M., Entin, J.K., Walker, J.P., Lohmann,
704 D., Toll, D., 2004. The global land data assimilation system. B. Am. Meteorol. Soc.
705 85, 381-394, http://dx.doi.org/10.1175/bams-85-3-381

706 Rossi, C.G., Srinivasan, R., Jirayoot, K., Duc, T.L., Souvannabouth, P., Binh, N., Gassman,
707 P.W., 2009. Hydrologic evaluation of the Lower Mekong River Basin with the soil
708 and water assessment tool model. IAEJ 18, 1-13,
709 http://114.255.9.31/iaej/EN/Y2009/V18/I01-02/1

710 Sabo, J.L., Ruhi, A., Holtgrieve, G.W., Elliott, V., Arias, M.E., Ngor, P.B., Räsänen, T.A.,
711 Nam, S., 2017. Designing river flows to improve food security futures in the
712 Lower Mekong Basin. Science 358, http://dx.doi.org/10.1126/science.aao1053

713 Spruce, J., Bolten, J.D., Srinivasan, R., 2017. Developing land use land cover maps for the
714 Lower Mekong Basin to aid SWAT hydrologic modeling, in: 2017 AGU Fall
715 Meeting, Abstract H104-298677. AGU, New Orleans, Louisiana.

716 Srinivasan, R., Arnold, J.G., Jones, C.A., 1998a. Hydrologic modelling of the United States
717 with the soil and water assessment tool. Int. J. Water Resour. D. 14, 315-325,
718 http://dx.doi.org/10.1080/07900629849231

719 Srinivasan, R., Ramanarayanan, T.S., Arnold, J.G., Bednarz, S.T., 1998b. Large area
720 hydrologic modeling and assessment part II: Model application. J. Am. Water
721 Resour. As. 34, 91-101, http://dx.doi.org/10.1111/j.1752-1688.1998.tb05962.x

722 Thanh, D.D., Cochrane, T.A., Arias, M.E., Tri, V.P.D., Vries, T.D., 2015. Analysis of water
723 level changes in the Mekong floodplain impacted by flood prevention systems
724 and upstream dams, in: The 36th IAHR World Congress. Hague, Netherlands.

725 Veilleux, J.C., Anderson, E.P., 2016. 2015 Snapshot of water security in the Nile, Mekong,
726 and Amazon River Basins. Limnol. Oceanogr.-Bull. 25, 8-14,
727 http://dx.doi.org/10.1002/lob.10085

728 Vörösmarty, C.J., McIntyre, P.B., Gessner, M.O., Dudgeon, D., Prusevich, A., Green, P.,
729 Glidden, S., Bunn, S.E., Sullivan, C.A., Liermann, C.R., Davies, P.M., 2010. Global
730 threats to human water security and river biodiversity. Nature 467, 555-561,
731 http://dx.doi.org/10.1038/nature09440

732 Wang, C., 2017. Study on the adverse effects of hydropower development on
733 international shipping. IOP Conf. Ser.: Earth Environ. Sci. 61, 012063,
734 http://dx.doi.org/10.1088/1755-1315/61/1/012063

735 Wang, W., Lu, H., Ruby Leung, L., Li, H.Y., Zhao, J., Tian, F., Yang, K., Sothea, K., 2017a.
736 Dam construction in Lancang‐Mekong River Basin could mitigate future flood
737 risk from warming‐induced intensified rainfall. Geophys. Res. Lett. 44, 10378-
738 10386, http://dx.doi.org/10.1002/2017GL075037

739 Wang, W., Lu, H., Yang, D., Sothea, K., Jiao, Y., Gao, B., Peng, X., Pang, Z., 2016.
740 Modelling Hydrologic Processes in the Mekong River Basin Using a Distributed
741 Model Driven by Satellite Precipitation and Rain Gauge Observations. PLOS ONE
742 11, e0152229, http://dx.doi.org/10.1371/journal.pone.0152229

743 Wang, W., Lu, H., Zhao, T., Jiang, L., Shi, J., 2017b. Evaluation and comparison of daily
744 rainfall from latest GPM and TRMM products over the Mekong River Basin. IEEE
745 J. Sel. Top. Appl. 10, 2540-2549, http://dx.doi.org/10.1109/JSTARS.2017.2672786

746 Weron, R., 2002. Estimating long-range dependence: Finite sample properties and
747 confidence intervals. Physica A 312, 285-299, http://dx.doi.org/10.1016/S0378-
748 4371(02)00961-5

749 Wild, T.B., Loucks, D.P., 2014. Managing flow, sediment, and hydropower regimes in the
750 Sre Pok, Se San, and Se Kong Rivers of the Mekong basin. Water Resour. Res. 50,
751 5141-5157, http://dx.doi.org/10.1002/2014WR015457

752 Winemiller, K.O., McIntyre, P.B., Castello, L., Fluet-Chouinard, E., Giarrizzo, T., Nam, S.,
753 Baird, I.G., Darwall, W., Lujan, N.K., Harrison, I., Stiassny, M.L.J., Silvano, R.A.M.,
754 Fitzgerald, D.B., Pelicice, F.M., Agostinho, A.A., Gomes, L.C., Albert, J.S., Baran, E.,
755 Petrere, M., Zarfl, C., Mulligan, M., Sullivan, J.P., Arantes, C.C., Sousa, L.M.,
756 Koning, A.A., Hoeinghaus, D.J., Sabaj, M., Lundberg, J.G., Armbruster, J., Thieme,
757 M.L., Petry, P., Zuanon, J., Vilara, G.T., Snoeks, J., Ou, C., Rainboth, W., Pavanelli,
758 C.S., Akama, A., Soesbergen, A.v., Sáenz, L., 2016. Balancing hydropower and
759 biodiversity in the Amazon, Congo, and Mekong. Science 351, 128-129,
760 http://dx.doi.org/10.1126/science.aac7082

761 WLE, Dataset on the dams of the Irrawaddy, Mekong, Red and Salween River Basins,
762 2017. https://wle-mekong.cgiar.org/maps/

763 Zhang, B., Zhang, L., Guo, H., Leinenkugel, P., Zhou, Y., Li, L., Shen, Q., 2014. Drought
764 impact on vegetation productivity in the Lower Mekong Basin. Int. J. Remote
765 Sens. 35, 2835-2856, http://dx.doi.org/10.1080/01431161.2014.890298

766 Ziv, G., Baran, E., Nam, S., Rodríguez-Iturbe, I., Levin, S.A., 2012. Trading-off fish
767 biodiversity, food security, and hydropower in the Mekong River Basin. P. Natl.
768 Acad. Sci. USA 109, 5609-5614, http://dx.doi.org/10.1073/pnas.1201423109
769

8. Table Titles

1. Streamflow regime variables used to assess the Lower Mekong flow changes.
2. The Lower Mekong River annual discharge statistics. Discharge units are in m^3/sec. Country codes are: CN (China), TH (Thailand), LA (Laos, PDR), and KH (Cambodia). The drainage area units are in square kilometers. The Q_{min} and Q_{max} refer to the minimum and the maximum annual discharge over the record at each site. The Q_1, Q_2, and Q_3 refer to the 25th, 50th (median), and 75th percentile of the mean annual discharge at each site. The μ refers to the mean annual discharge over the record, σ is the unbiased standard deviation, *CV* is the coefficient of variation, γ is the skewness, *H* is the Hurst coefficient (Hurst, 1951; Weron, 2002). The coefficient of variation CV is equal to σ/μ.
3. Parameters and calibrated values used for the LMRB model simulations. The identifier code refers to replace (V), addition (A), and multiplication (R).
4. Annual DAYCV analyses at the LMRB during the 2001–2015 time period. The $DAYCV_{\mu}$ column is the arithmetic mean of the annual DAYCV in percent. Values in parentheses refer to mean annual DAYCV during the 1960–2015 time period. Sub-basin 7 and 8 streamflow time record is different than the rest of the Sub-basin streamflow record as listed in Table 2. UMRB input adjustment scenarios simulation discharge time period is 2001–2015. Country codes are similar to descriptions in Table 2.
5. Seven-day maximum flow at the LMRB during 2001–2015 Mann Kendall trend analysis. The μ is the arithmetic mean of the seven-day maximum flow (*7QMAX*)

792 in millimeter per day, τ (tau) is Kendall's tau correlation coefficient, p-value is 2
793 sided-test, and trend is Significant when ($p \leq 0.05$). Country codes are similar to
794 descriptions in Table 2.

795 A. 1. Dams data within the Mekong Basin obtained from CGIAR (WLE, 2017). Country
796 codes are similar to descriptions in Table 2 with the addition of *VN* as Viet Nam. The
797 COD column refers to the Commercial Operation Date (i.e. when the dam was
798 commissioned).

9. Figure Captions

1. (a) The Lower Mekong River Basin. Streamflow gauges follow the Lower Mekong River Basin subareas presented by *Rossi et al.,* (2009). Cities with population classes obtained from Environmental Systems Research Institute, Inc. (ESRI) World Populated Places layer (https://www.arcgis.com/home/index.html, accessed on 31 May 2018) are depicted in red (greater than 5 million), orange (1-5 million), and light green (0.5-1 million). Land use and land cover class descriptions are shown in Figure 1-(b). Dam data are described in Appendix A.1 and Table A. 1. (b) Land use and land cover class descriptions as depicted in Figure 1-(a).
2. Lower Mekong basin time series data. Annual precipitation in millimeters (colored in blue), mean annual maximum air temperature (colored in black) in degrees Celsius, and mean annual minimum air temperature (colored in black) in degrees Celsius time series data are aggregated over the entire Lower Mekong basin.
3. Daily simulated and observed discharge in m^3/sec for the Lower Mekong River at six sub-basin watersheds as presented in Figure 1 in calibration of the LMRB model. The LMRB model calibration years are 2005 and 2006. The percent error (Q_{err}) between daily simulated and observed discharge and the Nash–Sutcliffe (NSE) performance metrics are depicted for each sub-basin.
4. Monthly mean observed and simulated discharge (m^3/sec) for the Lower Mekong River at six sub-basin watersheds as presented in Figure 1 in calibration

821 of the LMRB model. The LMRB model calibration years are 2005 and 2006. The
822 percent error (Qerr) between monthly mean simulated and observed discharge
823 and the Nash–Sutcliffe (NSE) performance metrics are depicted for each sub-
824 basin.
825 5. Scatterplot of monthly observed and simulated discharge in m^3/sec for the
826 Lower Mekong River at six sub-basin watersheds in validation of the LMRB model
827 during 2001–2004, and 2007–2015. The Nash–Sutcliffe (NSE) performance
828 metrics during validation time period are depicted for each sub-basin.
829 6. Vientiane (SB3) hydrograph. Mean, minimum, and maximum daily discharge
830 during 1913–2016.
831 7. Sensitivity analysis for the Lower Mekong River Basin Colwell index predictability
832 (*P*). Observed predictability during 2001–2015 time period at SB4, SB5, and SB6
833 is 0.342, 0.325, 0.317 respectively. Predictability change from observed
834 predictability depicted in y-axis at each panel were calculated from simulated
835 flow obtained by driving the LMRB model with adjusted Upper Mekong River
836 flow inputs during the 2001-2015 time period as outlined in x-axis. Predictability
837 change (y-axis) reports the scaled predictability change, i.e., $(P_{sim} - P_{obs})/$
838 $P_{obs} \times 100$. Sub-basin watersheds follow description in Figure 1.
839 8. Colwell index, Predictability (*P*), Constancy (*C*), and Contingency (*M*) of
840 streamflow for the Lower Mekong River Basin. Data for current streamflow
841 status Colwell predictability analyses are daily discharge for the years 2001–
842 2015. Flow simulations for different scenarios predictability analyses were

obtained by driving the LMRB model with adjusted UMRB flow inputs during the 2001-2015 time period. Sub-basin watersheds follow description in Figure 1.

9. Annual flow reversal analyses at the LMRB. Black line gives flow reversals (*FLOWREV*) in days for the time period of 1960–2015 calculated from observed discharge, blue line gives (*FLOWREV*) calculated from simulated discharge with the UMRB inflow increased by 30%, and red line gives (*FLOWREV*) calculated from simulated discharge with the UMRB inflow decreased by 30%. Simulation discharge time period is 2001–2015 highlighted in grey. Sub-basin watersheds follow description in Figure 1.
10. Flood duration (*FLDDUR*) analyses at the LMRB. The flood duration in days are the number of days when discharge equals or exceeds a threshold discharge magnitude causing floods. Black bars give flood duration in days for the 1960–2015 time period calculated from observed discharges, and blue bars give flood duration calculated from simulated discharges with the UMRB inflow increased by 30%. Simulation discharge time period is 2001–2015 highlighted in gray. Sub-basin watersheds follow description in Figure 1.

859 Table 1. Streamflow regime variables used to assess the Lower Mekong flow changes.

Variable name	Acronym	Definition	Streamflow classification
Coefficient of variation	*DAYCV*	The ratio of the standard deviation of daily flows to the average of daily flows multiplied by 100 during a calendar year	Flow variability and predictability
Flow reversal	*FLOWREV*	The average number of daily flow reversals per year	
Colwell index of Predictability	*P*	Predictability of flow using an index developed by Colwell [1974] which is based on information theory	
Colwell index of Constancy	*C*		
Colwell index of Contingency	*M*		
Flood duration	*FLDDUR*	The average number of days per year when flow equals or exceeds *flood threshold*	High flow disturbance
7 day maximum flow	*7QMAX*	The average annual maxima of 7 day means of daily mean streamflow	

860

Table 2. The Lower Mekong River annual discharge statistics. Discharge units are in m^3/sec. Country codes are: CN (China), TH (Thailand), LA (Laos, PDR), and KH (Cambodia). The drainage area units are in square kilometers. The Q_{min} and Q_{max} refer to the minimum and the maximum annual discharge over the record at each site. The Q_1, Q_2, and Q_3 refer to the 25th, 50th (median), and 75th percentile of the mean annual discharge at each site. The μ refers to the mean annual discharge over the record, σ is the unbiased standard deviation, *CV* is the coefficient of variation, γ is the skewness, *H* is the Hurst coefficient (Hurst, 1951; Weron, 2002). The coefficient of variation CV is equal to σ/μ.

Station Name	Code	Country	LMRB	Start Date	End Date	Drainage Area	Q_{min}	Q_1	Q_2	Q_3	Q_{max}	μ	σ	*CV*	γ	*H*
Chinese Border	010000	CN	Upper basin inlet	1/1/1985	12/31/2007	—	1,619	2,010	2,157	2,459	2,763	2,221	303	0.14	0.03	0.35
Chiang Sean	010501	TH	Sub-basin 1 outlet	1/1/1960	12/31/2016	191,055	1,871	2,304	2,564	2,929	4,027	2,618	427	0.16	0.60	0.72
Luang Prabang	011201	LA	Sub-basin 2 outlet	1/1/1939	12/31/2016	273,838	1,852	3,410	3,754	4,177	5,488	3,777	707	0.19	-0.12	0.70
Vientiane	011901	LA	Sub-basin 3 outlet	1/1/1913	12/31/2016	303,528	2,677	3,975	4,455	4,900	6,111	4,476	710	0.16	0.10	0.67
Mukdahan	013402	TH	Sub-basin 4 outlet	1/1/1923	12/31/2016	394,134	5,256	7,246	8,031	9,012	10,496	8,071	1,168	0.14	-0.02	0.89
Pakse	013901	LA	Sub-basin 5 outlet	1/1/1923	12/31/2016	550,955	6,835	9,095	10,050	11,165	12,918	10,066	1,434	0.14	-0.08	0.68
Kratie	014901	KH	Sub-basin 6 outlet	1/1/1924	12/31/2016	656,518	6,599	11,891	13,527	15,077	19,562	13,411	2,591	0.19	-0.41	0.77
Yasothom	370104	TH	Sub-basin 7 outlet	1/1/1952	12/31/2003	46,805	77	171	240	287	602	242	102	0.42	1.21	0.60
Rasi Salai	380134	TH	Sub-basin 8 outlet	1/1/1979	12/31/2003	43,878	5	95	154	223	447	177	107	0.60	0.79	0.94

868 Table 3. Parameters and calibrated values used for the LMRB model simulations. The identifier code refers to replace (V), addition
869 (A), and multiplication (R).

	Parameter	Description	Range	Identifer code	Calibrated Value
Precipitation					
	PRECIPITATION	Correction factor to grid precipitation record	-1, +0.01	R	-0.445 to +0.00225
High Flow					
	CN2	Intiial SCS runoff curve number to moisture condition II	-0.1, +0.1	R	-0.07
	AWC	Available water capacity of the soil layer	-0.1, +0.1	R	+0.07
	ESCO	Soil evaportaion compensation factor	+0.5, +0.9	V	+0.6
Base Flow					
	GWHT	Initial groundwater height	0, +1.0	V	+0.075
	GW_DELAY	Groundwater delay time	-30, +60	A	-14.25
	GWQMN	Threshold depth of water in the shallow aquifer	-1000, +1000	A	-450
	REVAPMN	Percolation to the deep aquifer to occur	-750, +750	A	+262.5
	GW_REVAP	Groundwater "revap" coefficient	+0.02, +0.10	V	+0.042
	RCHRG_DP	Deep aquifer percolation fraction	-0.05, +0.05	A	+0.0375

870

871

Table 4. Annual DAYCV analyses at the LMRB during the 2001–2015 time period. The $DAYCV_{\mu}$ column is the arithmetic mean of the annual DAYCV in percent. Values in parentheses refer to mean annual DAYCV during the 1960–2015 time period. Sub-basin 7 and 8 streamflow time record is different than the rest of the Sub-basin streamflow record as listed in Table 2. UMRB input adjustment scenarios simulation discharge time period is 2001–2015. Country codes are similar to descriptions in Table 2.

No.	LMRB	Station Name	Country	Code	$DAYCV_{\mu}$
1	Sub-basin 1 outlet	Chiang Sean	TH	010501	70.10 (76.52)
2	Sub-basin 2 outlet	Luang Prabang	LA	011201	80.73 (82.85)
3	Sub-basin 3 outlet	Vientiane	LA	011901	81.83 (84.51)
4	Sub-basin 4 outlet	Mukdahan	TH	013402	88.57 (93.56)
5	Sub-basin 5 outlet	Pakse	LA	013901	95.38 (97.25)
6	Sub-basin 6 outlet	Kratie	KH	014901	93.41 (95.68)
7	Sub-basin 7 outlet	Yasothom	TH	370104	(116.68)
8	Sub-basin 8 outlet	Rasi Salai	TH	380134	(154.31)
Inputs from Upper Mekong increased by 30%					
1	Sub-basin 1 outlet	Chiang Sean	TH	010501	84.46
2	Sub-basin 2 outlet	Luang Prabang	LA	011201	90.89
3	Sub-basin 3 outlet	Vientiane	LA	011901	94.53
4	Sub-basin 4 outlet	Mukdahan	TH	013402	100.84
5	Sub-basin 5 outlet	Pakse	LA	013901	93.99
6	Sub-basin 6 outlet	Kratie	KH	014901	91.69
7	Sub-basin 7 outlet	Yasothom	TH	370104	84.48
8	Sub-basin 8 outlet	Rasi Salai	TH	380134	91.05
Inputs from Upper Mekong decreased by 30%					
1	Sub-basin 1 outlet	Chiang Sean	TH	010501	68.45
2	Sub-basin 2 outlet	Luang Prabang	LA	011201	78.90
3	Sub-basin 3 outlet	Vientiane	LA	011901	86.10
4	Sub-basin 4 outlet	Mukdahan	TH	013402	97.92
5	Sub-basin 5 outlet	Pakse	LA	013901	91.54
6	Sub-basin 6 outlet	Kratie	KH	014901	90.25
7	Sub-basin 7 outlet	Yasothom	TH	370104	84.48
8	Sub-basin 8 outlet	Rasi Salai	TH	380134	91.05

Table 5. Seven-day maximum flow at the LMRB during 2001–2015 Mann Kendall trend analysis. The μ is the arithmetic mean of the seven-day maximum flow (*7QMAX*) in millimeter per day, τ (tau) is Kendall's tau correlation coefficient, p-value is 2 sided-test, and trend is Significant when ($p \leq 0.05$). Country codes are similar to descriptions in Table 2.

LMRB	Sub-basin 1 outlet	Sub-basin 2 outlet	Sub-basin 3 outlet	Sub-basin 4 outlet	Sub-basin 5 outlet	Sub-basin 6 outlet
Station Name	Chiang Sean	Luang Prabang	Vientiane	Mukdahan	Pakse	Kratie
Country	TH	LA	LA	TH	LA	KH
Code	010501	011201	011901	013402	013901	014901
μ	3.3	3.8	4.0	6.1	5.3	6.0
τ, tau	-0.486	-0.219	-0.410	-0.314	-0.333	-0.352
p-Value	0.013	0.276	0.038	0.113	0.092	0.075
Trend	Significant	No Trend	Significant	No Trend	No Trend	No Trend
Inputs from Upper Mekong increased by 30%						
μ	4.2	3.7	4.1	6.1	4.9	5.9
τ, tau	-0.390	-0.333	-0.352	-0.029	-0.124	-0.029
p-Value	0.048	0.092	0.075	0.921	0.553	0.921
Trend	Significant	No Trend	No Trend	No Trend	No Trend	No Trend
Inputs from Upper Mekong decreased by 30%						
μ	2.8	2.7	3.2	5.5	4.5	5.5
τ, tau	-0.314	-0.219	-0.200	0.048	0.067	0.105
p-Value	0.113	0.276	0.322	0.843	0.767	0.621
Trend	No Trend	No Trend	No Trend	No Trend	No Trend	No Trend

Table A. 1. Dams data within the Mekong Basin obtained from CGIAR (WLE, 2017). Country codes are similar to descriptions in Table 2 with the addition of *VN* as Viet Nam. The COD column refers to the Commercial Operation Date (i.e. when the dam was commissioned).

No	Name	Country	River	Latitude	Longitude	Function	Status	COD	Installed capacity	Mean annual energy	Height	Crest length	Full supply level	Max reservoir area	Est. cost	Power destination (%)							Developers	Owner/ operator	Notes
								Year	Megawatts	Gigawatts	meter	meter	Million m^3	km^2	Mil. US$	LAO	THA	CAM	VN	CHN	MYN	IND			
1	Lower Sesan 2	KH	Se San	13° 33' 5"	106° 15' 50"	Hydropower	Under construction	2019	480	2,311.8	45	7,729	1,790	335	781.52	0	0	30	70	0	0	0	HydroLancang and Royal Group		Location derived from Sesan, Sre Pok, and Sekong (3Ss) River Basins Development Study in Kingdom of Cambodia, Lao People's Democratic Republic, and Socialist Republic of Viet Nam. ADB - RETA 40082.
2	Nam Ngum 1	LA	Nam Ngum	18° 31' 52"	102° 32' 51"	Hydropower	Commissioned	1971	149	1,006.00	75	468	4,700	370	97	80	20	0	0	0	0	0		EdL Gen (100%)	
3	Nam Theun 2	LA	Nam Theun	17° 59' 50"	104° 57' 8"	Hydropower	Commissioned	2009	1075	5,936.00	48	325	3,500	450	1300	7	93	0	0	0	0	0		Nam Theun Power Co. (EDF: 40%; EGCO (Thailand): 35%; GoL: 25%)	
4	Siridhorn	TH	Lam Dom Noi	15° 12' 23"	105° 25' 45"	Hydropower	Commissioned	1971	36	86.00	42	940	1,967	288		0	100	0	0	0	0	0			
5	Ubol Ratana	TH	Nam Pong	16° 46' 31"	102° 37' 6"	Hydropower	Commissioned	1966	25.2	57.00	35.1	885	2,559	410		0	100	0	0	0	0	0	Electricity Generating Authority of Thailand	Electricity Generating Authority of Thailand	https://en.wikipedia.org/wiki/Ubol_Ratana_Dam
6	Dak N'Teng	VN	Dak N'Teng	12° 11' 46"	107° 55' 36"	Hydropower	Commissioned	2011	13	52.80	31	315	25.49	323		n/a	n/a	n/a	n/a	n/a	n/a	n/a			Data provided by IWRP

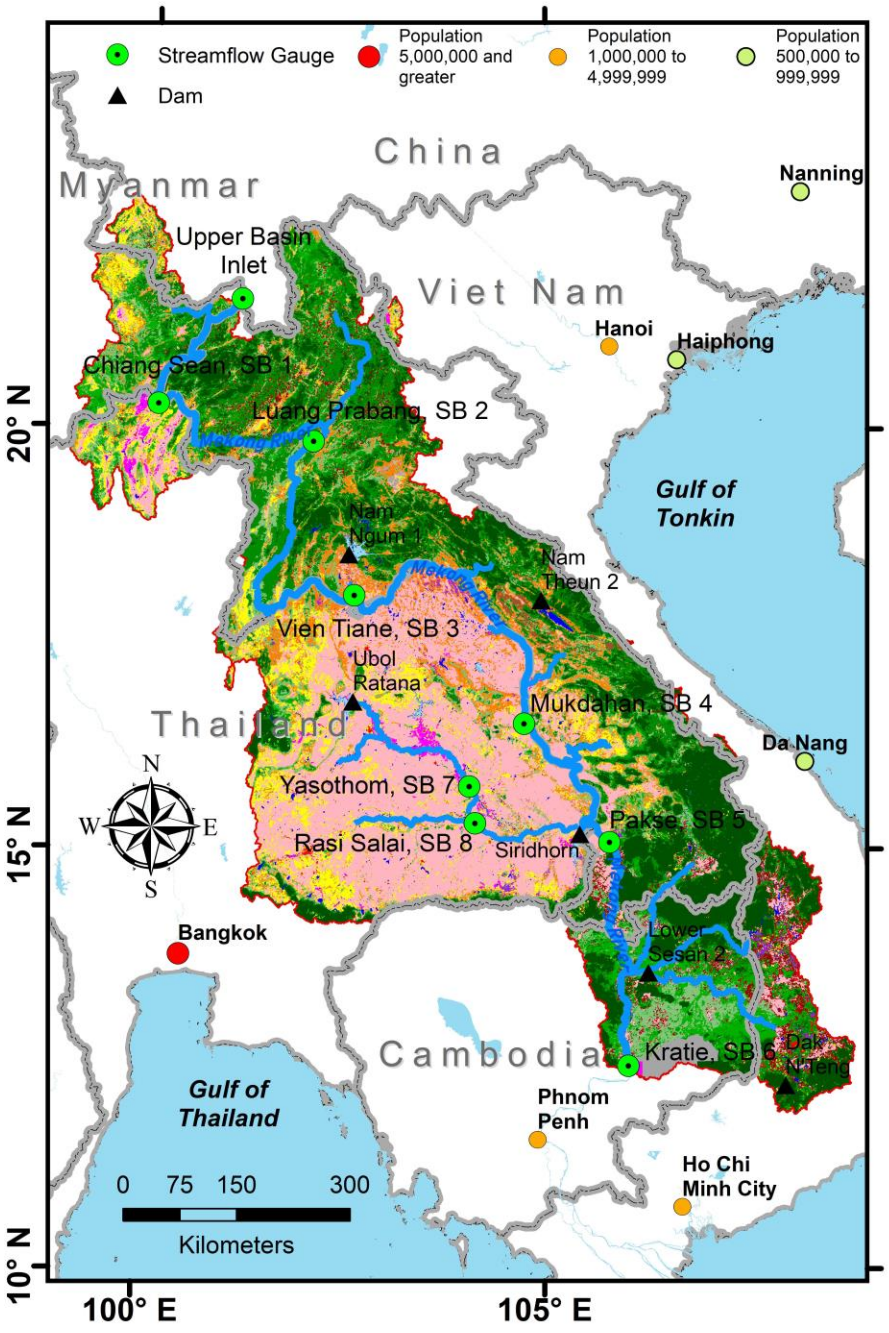

887

888 Figure 1. (a) The Lower Mekong River Basin. Streamflow gauges follow the Lower
889 Mekong River Basin subareas presented by *Rossi et al.,* (2009). Cities with population
890 classes obtained from Environmental Systems Research Institute, Inc. (ESRI) World
891 Populated Places layer (https://www.arcgis.com/home/index.html, accessed on 31 May
892 2018) are depicted in red (greater than 5 million), orange (1-5 million), and light green
893 (0.5-1 million). Land use and land cover class descriptions are shown in Figure 1-(b).
894 Dam data are described in Appendix A.1 and Table A. 1.

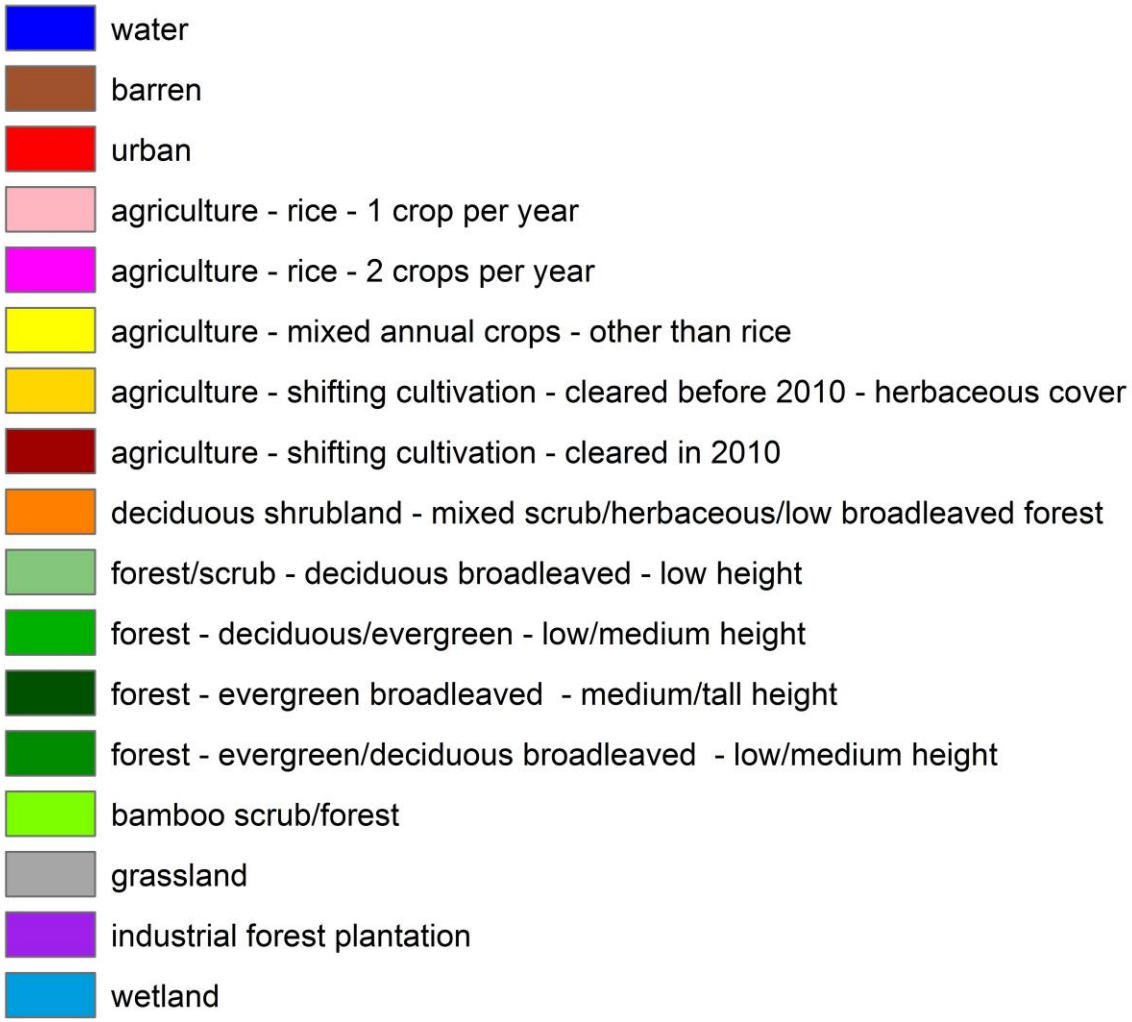

Figure 1. (b) Land use and land cover class descriptions as depicted in Figure 1-(a).

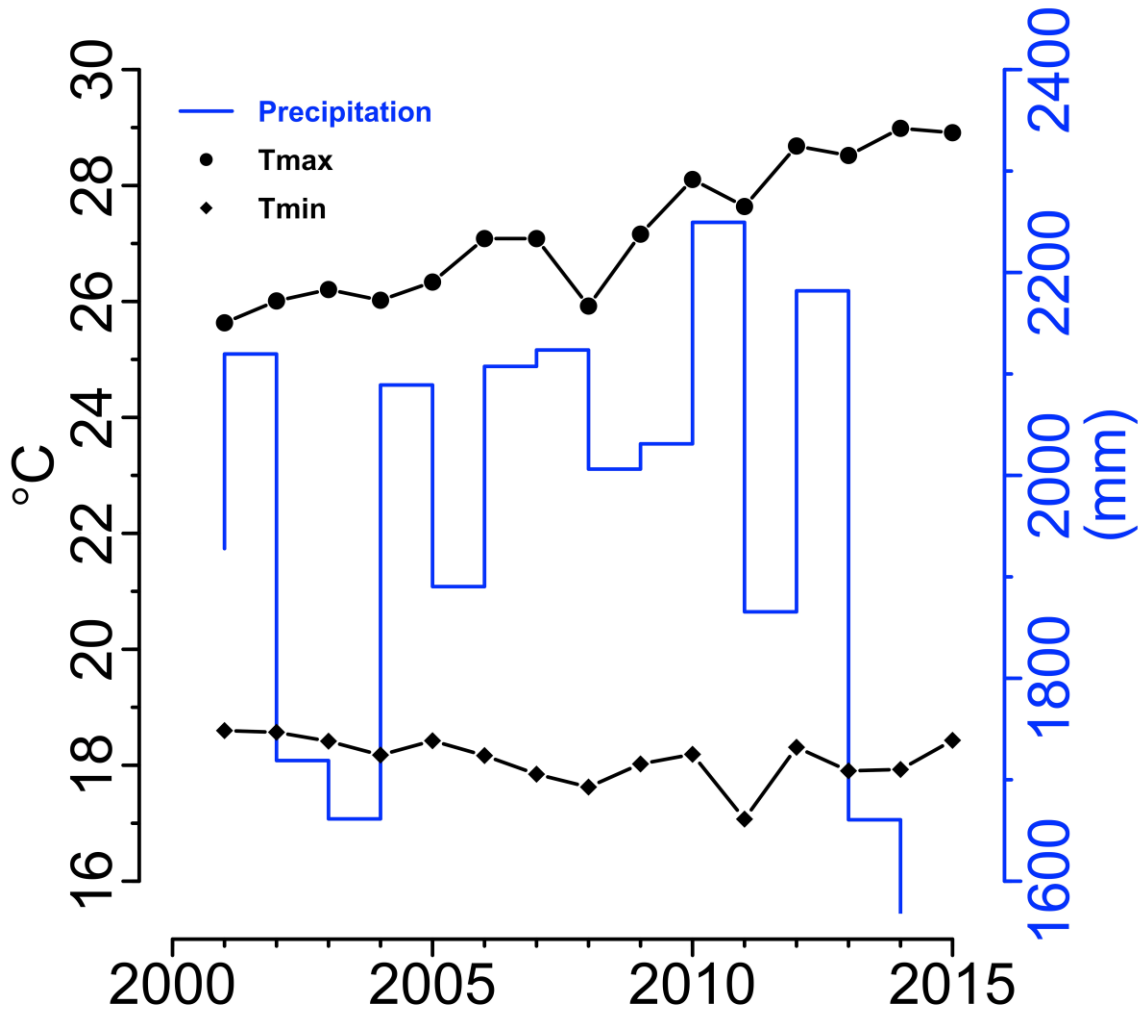

897

898 Figure 2. Lower Mekong basin time series data. Annual precipitation in millimeters
899 (colored in blue), mean annual maximum air temperature (colored in black) in degrees
900 Celsius, and mean annual minimum air temperature (colored in black) in degrees Celsius
901 time series data are aggregated over the entire Lower Mekong basin.

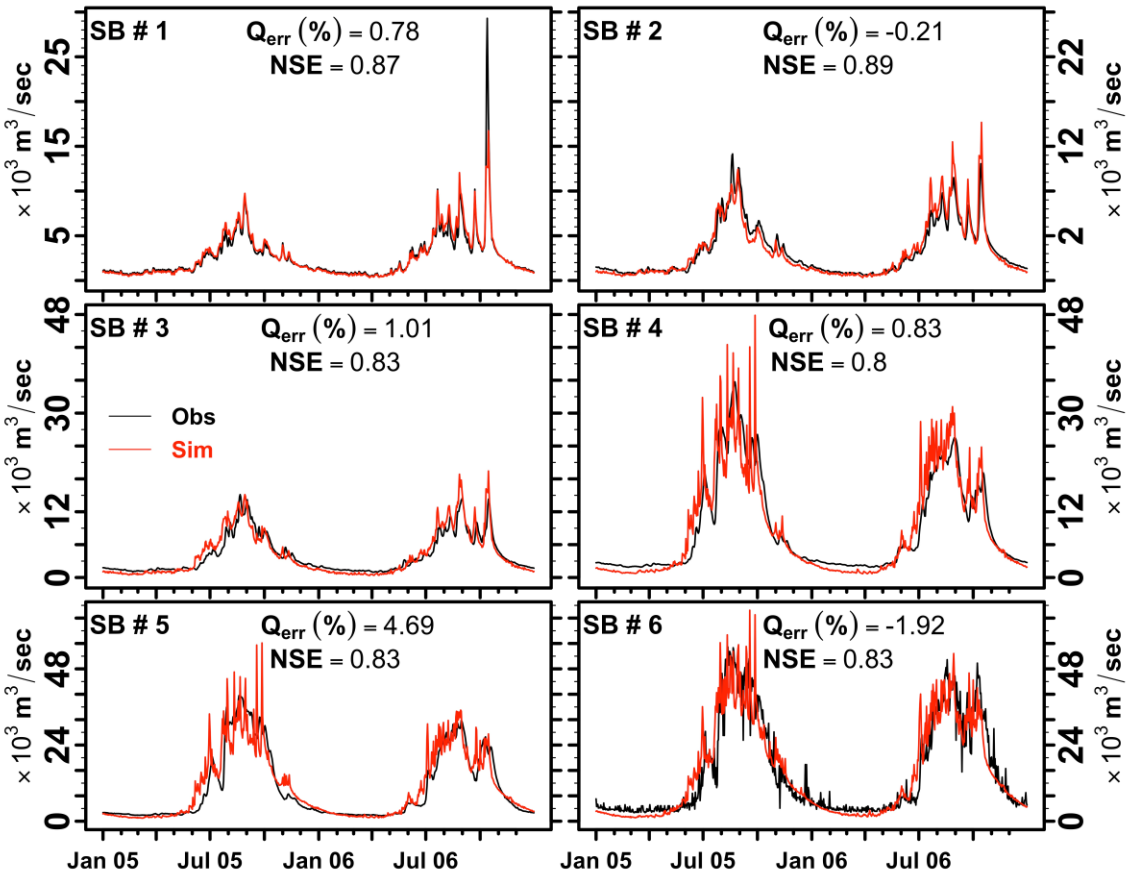

902

903 Figure 3. Daily simulated and observed discharge in m^3/sec for the Lower Mekong River
904 at six sub-basin watersheds as presented in Figure 1 in calibration of the LMRB model.
905 The LMRB model calibration years are 2005 and 2006. The percent error (Q_{err}) between
906 daily simulated and observed discharge and the Nash–Sutcliffe (NSE) performance
907 metrics are depicted for each sub-basin.

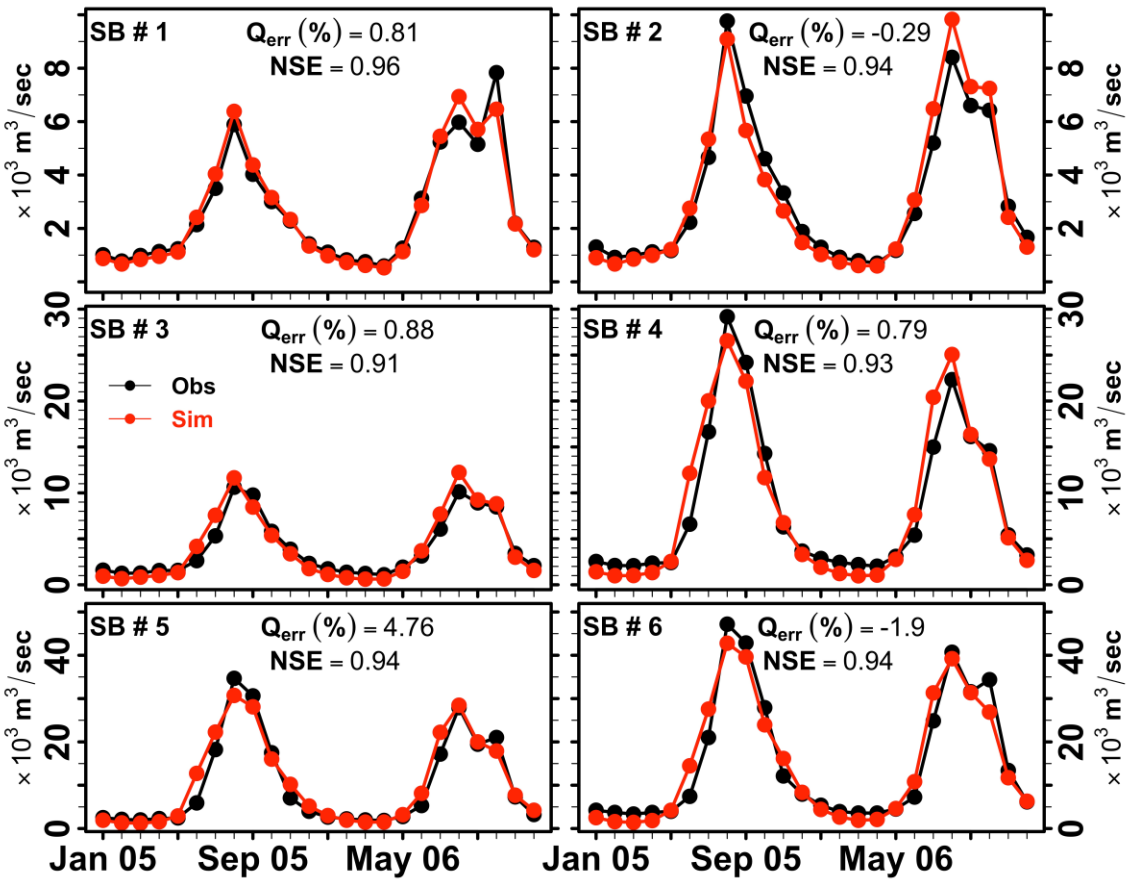

908

909 Figure 4. Monthly mean observed and simulated discharge (m^3/sec) for the Lower
910 Mekong River at six sub-basin watersheds as presented in Figure 1 in calibration of the
911 LMRB model. The LMRB model calibration years are 2005 and 2006. The percent error
912 (Qerr) between monthly mean simulated and observed discharge and the Nash–Sutcliffe
913 (NSE) performance metrics are depicted for each sub-basin.

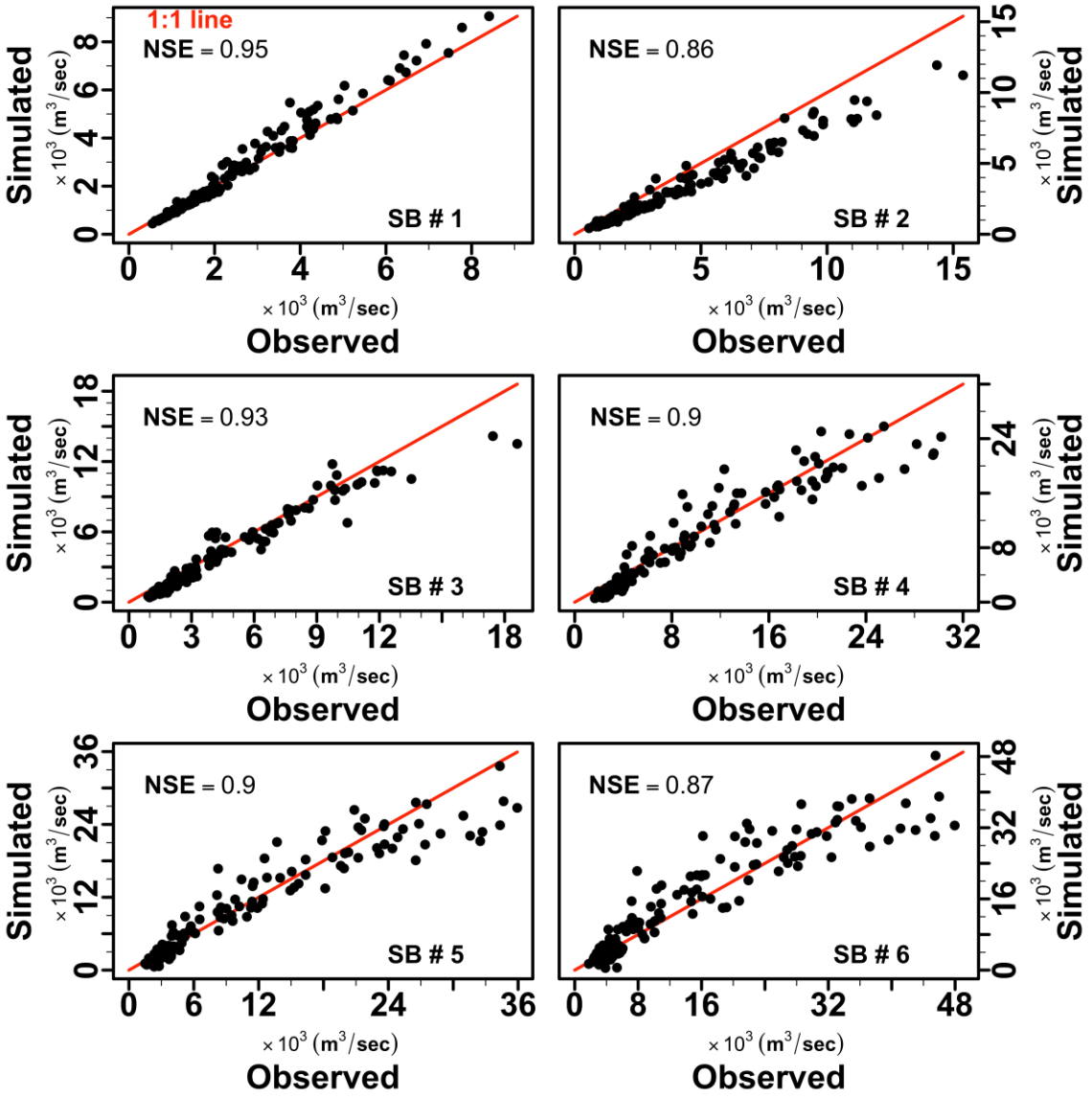

914

915 Figure 5. Scatterplot of monthly observed and simulated discharge in m^3/sec for the
916 Lower Mekong River at six sub-basin watersheds in validation of the LMRB model during
917 2001–2004, and 2007–2015. The Nash–Sutcliffe (NSE) performance metrics during
918 validation time period are depicted for each sub-basin.

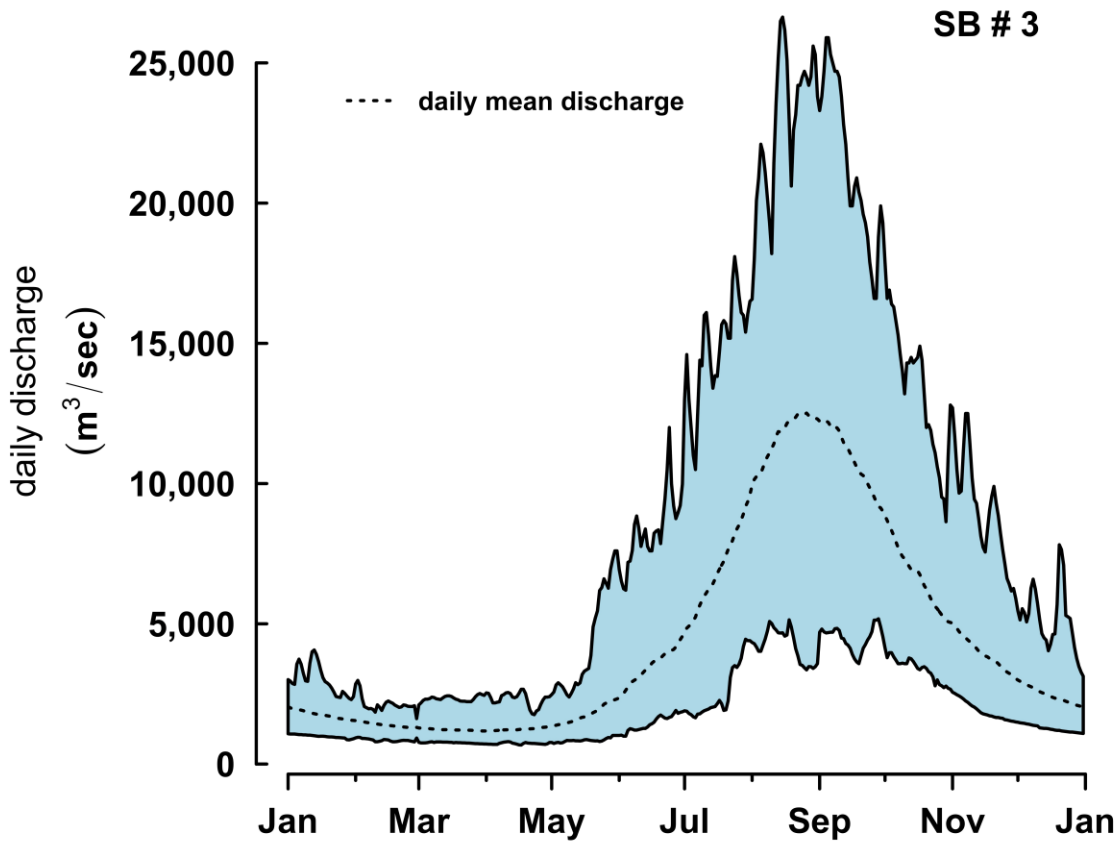

919

920 Figure 6. Vientiane (SB3) hydrograph. Mean, minimum, and maximum daily discharge
921 during 1913–2016.

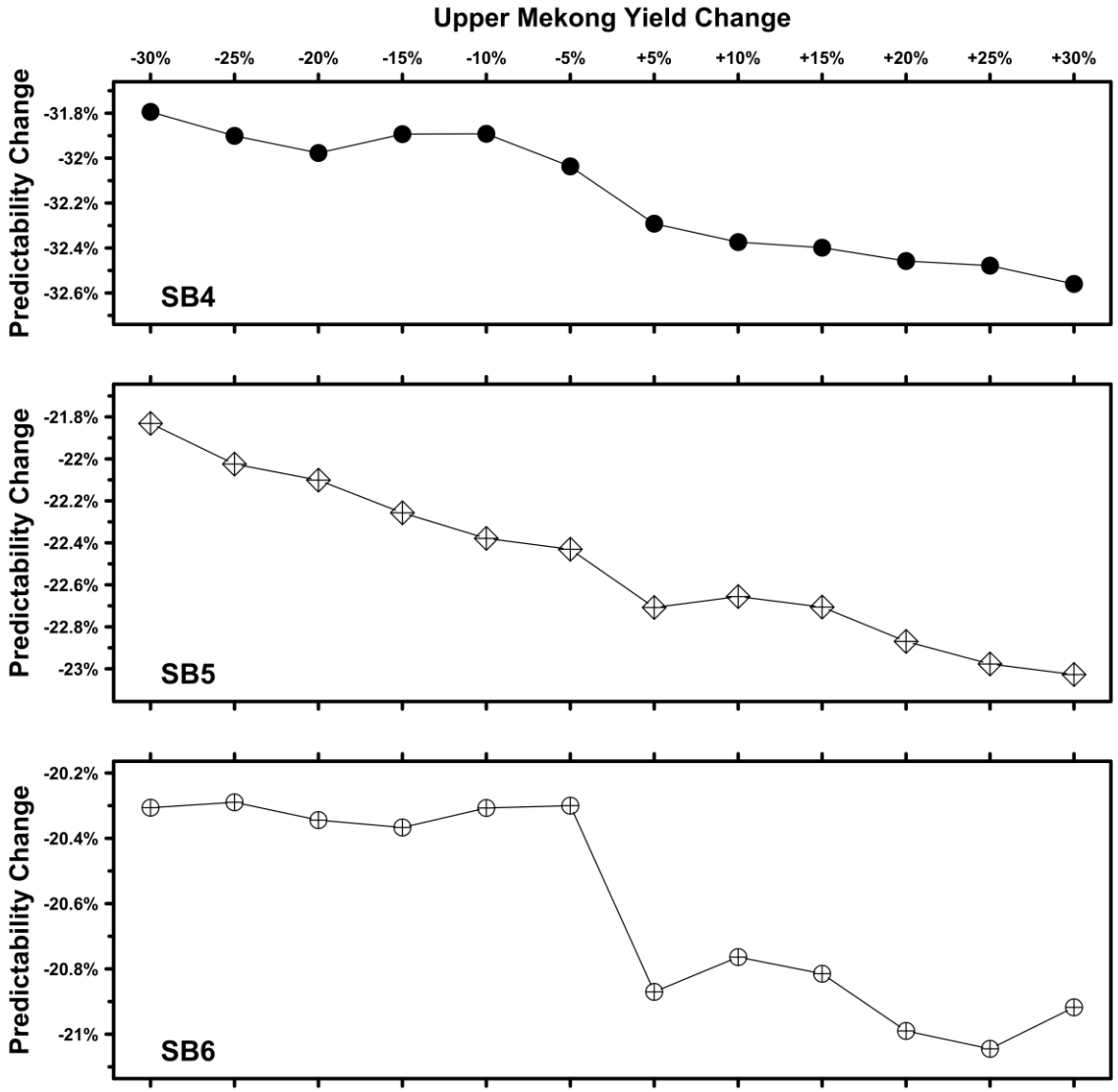

Figure 7. Sensitivity analysis for the Lower Mekong River Basin Colwell index predictability (*P*). Observed predictability during 2001–2015 time period at SB4, SB5, and SB6 is 0.342, 0.325, 0.317 respectively. Predictability change from observed predictability depicted in y-axis at each panel were calculated from simulated flow obtained by driving the LMRB model with adjusted Upper Mekong River flow inputs during the 2001-2015 time period as outlined in x-axis. Predictability change (y-axis) reports the scaled predictability change, i.e., $(P_{sim} - P_{obs})/P_{obs} \times 100$. Sub-basin watersheds follow description in Figure 1.

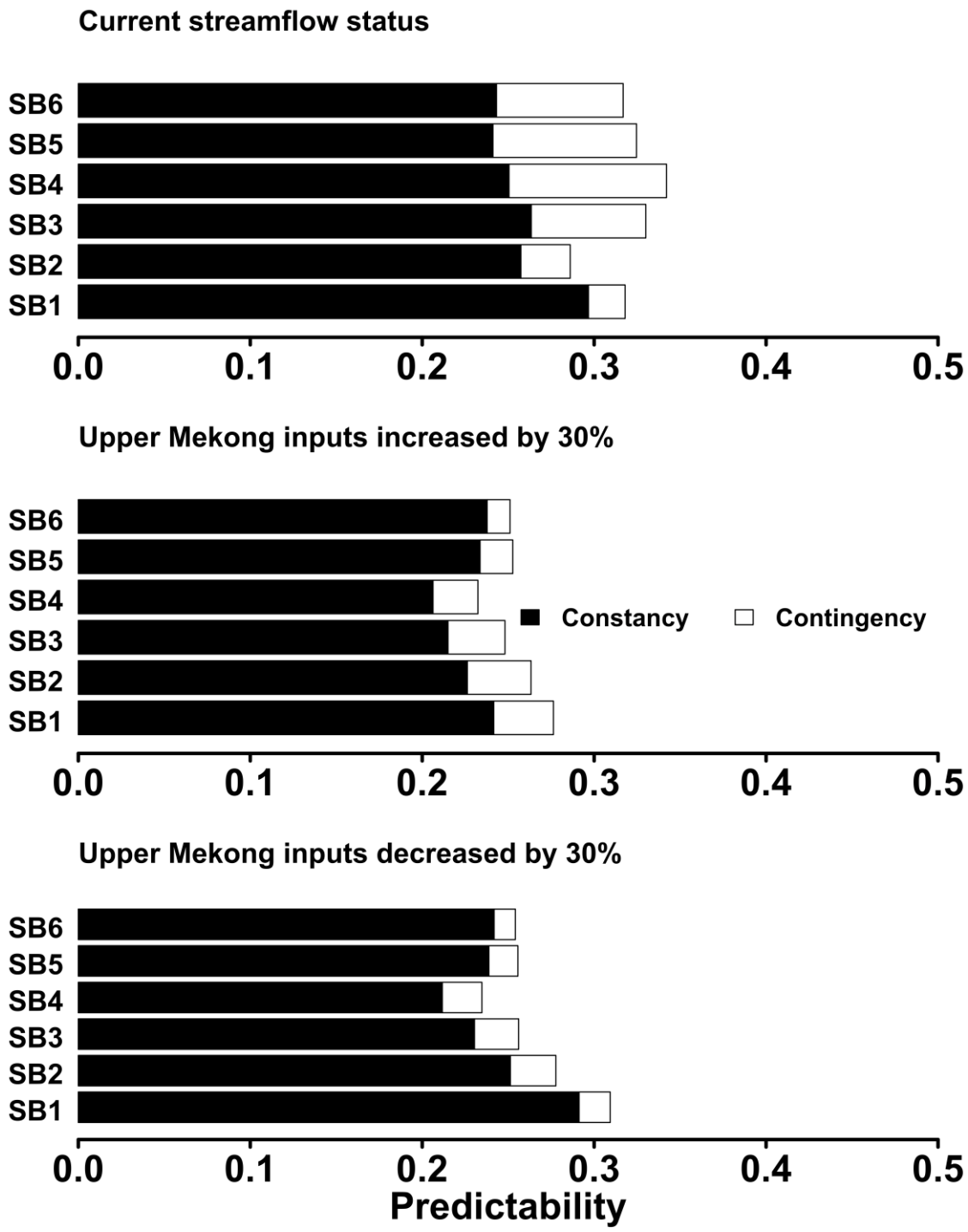

931

932 Figure 8. Colwell index, Predictability (*P*), Constancy (*C*), and Contingency (*M*) of
933 streamflow for the Lower Mekong River Basin. Data for current streamflow status
934 Colwell predictability analyses are daily discharge for the years 2001–2015. Flow
935 simulations for different scenarios predictability analyses were obtained by driving the
936 LMRB model with adjusted UMRB flow inputs during the 2001-2015 time period. Sub-
937 basin watersheds follow description in Figure 1.

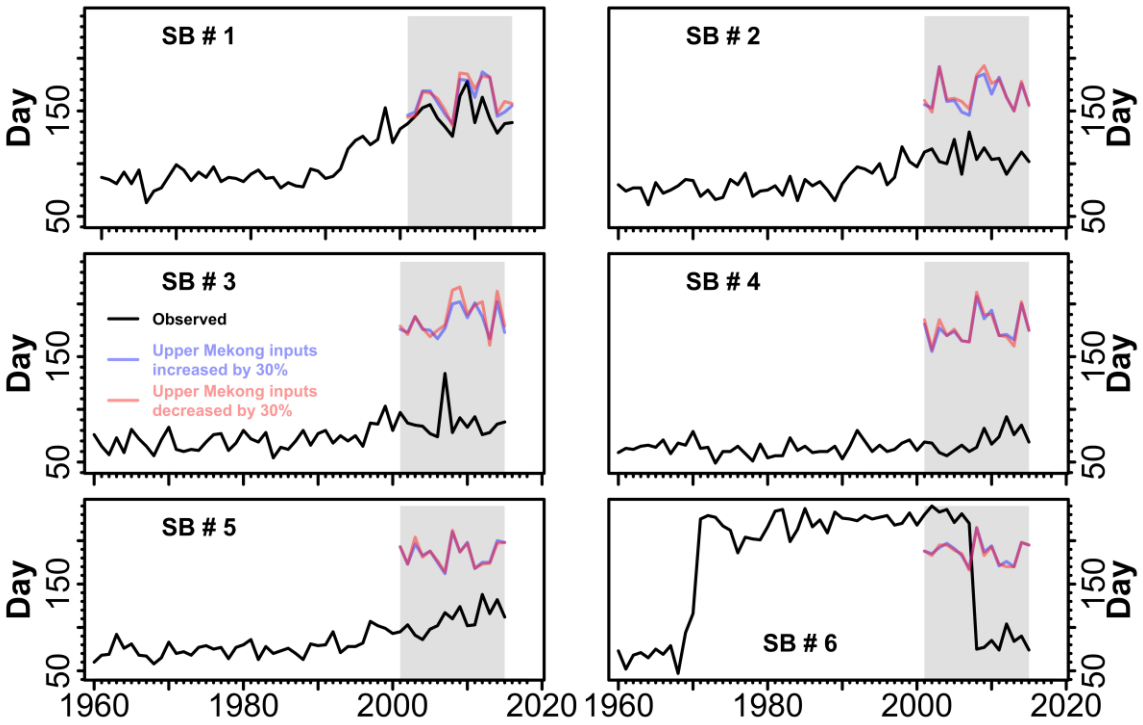

938

939 Figure 9. Annual flow reversal analyses at the LMRB. Black line gives flow reversals
940 (*FLOWREV*) in days for the time period of 1960–2015 calculated from observed
941 discharge, blue line gives (*FLOWREV*) calculated from simulated discharge with the
942 UMRB inflow increased by 30%, and red line gives (*FLOWREV*) calculated from simulated
943 discharge with the UMRB inflow decreased by 30%. Simulation discharge time period is
944 2001–2015 highlighted in grey. Sub-basin watersheds follow description in Figure 1.

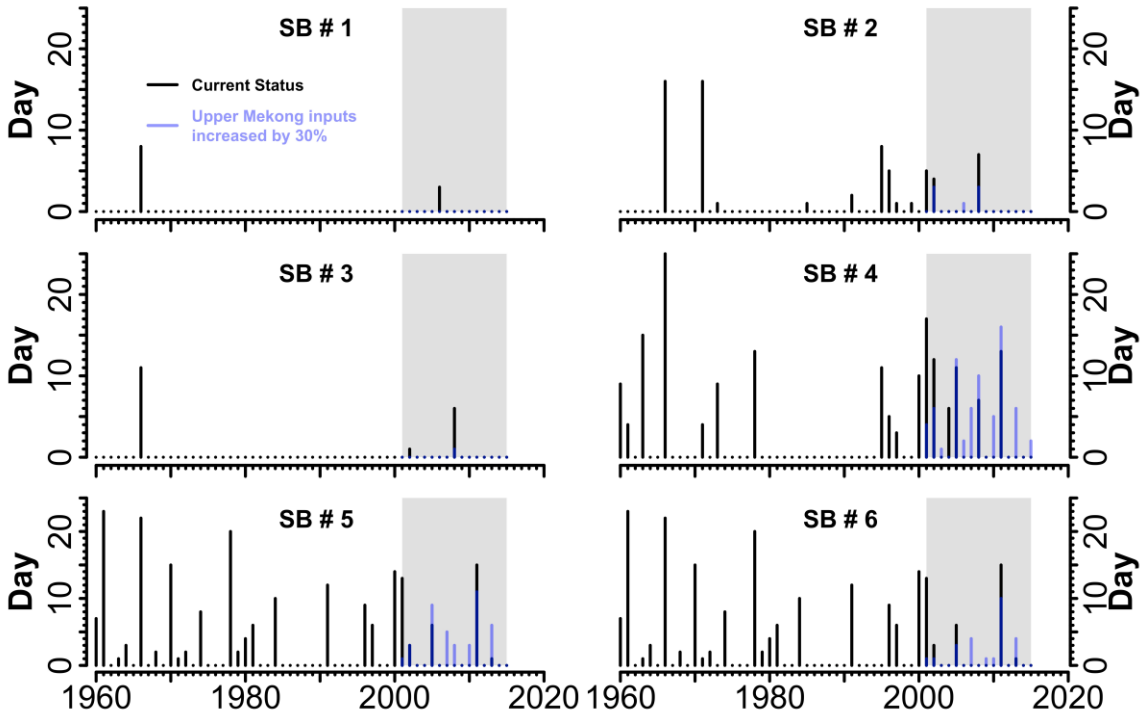

945

946 Figure 10. Flood duration (*FLDDUR*) analyses at the LMRB. The flood duration in days
947 are the number of days when discharge equals or exceeds a threshold discharge
948 magnitude causing floods. Black bars give flood duration in days for the 1960–2015
949 time period calculated from observed discharges, and blue bars give flood duration
950 calculated from simulated discharges with the UMRB inflow increased by 30%.
951 Simulation discharge time period is 2001–2015 highlighted in gray. Sub-basin
952 watersheds follow description in Figure 1.